Geochemistry of the Jurassic and upper Cretaceous shales from the Molango Region, Hidalgo, eastern Mexico: Implications for source-area weathering, provenance, and tectonic setting

John S. Armstrong-Altrin [a,*], Ramasamy Nagarajan [b], Jayagopal Madhavaraju [c], Leticia Rosalez-Hoz[a], Yong Il Lee[d], Vysetti Balaram[e], Adriana Cruz-Martinez[f] and Gladis Avila-Ramirez[g]

[a] *Unidad de Procesos Oceánicos y Costeros, Instituto de Ciencias del Mar y Limnología, Universidad Nacional Autónoma de México, Circuito Exterior s/n, 04510, México D.F., México*

[b] *Department of Applied Geology, School of Engineering and Science, Curtin University, CDT 250, 98009, Miri, Sarawak, Malaysia*

[c] *Estación Regional del Noroeste, Instituto de Geología, Universidad Nacional Autónoma de México, Hermosillo 83000, Sonora, México*

[d] *School of Earth and Environmental Sciences, Seoul National University, Seoul 151-747, Korea*

[e] *Geochemistry Division, National Geophysical Research Institute, Uppal Road, Hyderabad - 500606, India*

[f] *Itztepetl, Ciencias de la Tierra y Afines S.C., C.P. 42035, Pachuca, Hidalgo, Mexico.*

[g] *Licenciatura en Química, Universidad Autónoma del Estado de Hidalgo, Centro de Investigaciones en Ciencias de la Tierra, Ciudad Universitaria, Carretera Pachuca-Tulancingo Km. 4.5, 42184 Pachuca, Hidalgo, Mexico*

[*] Corresponding Author. Tel.: +52-55-56230222 Ext.: 45372; Fax: +52-55-56229766.

E-mail address: john_arms@yahoo.com; armstrong@cmarl.unam.mx (John S. Armstrong-Altrin)

Revised manuscript submitted to ***Comptes Rendus Geoscience, 13 February 2013***

ABSTRACT

The weathering conditions, provenance, and tectonic setting of shales from the Pimienta (PF; upper Jurassic), Huayacocotla (HF; lower Jurassic), and Méndez Formations (MF; upper Cretaceous) of the Molango Region, Hidalgo, Mexico have been studied for the first time using mineralogy, major, and trace element data. The X-ray diffraction (XRD) data reveals that the shales consist mostly of illite and muscovite clay minerals. The SEM-EDS study indicates that the PF and HF shales are rich in phosphate minerals and MF shales are abundant in zircon mineral. The chemical index of alteration (CIA ~ 59 to 93) and their position in the A-CN-K (Al_2O_3 - CaO + Na_2O - K_2O) ternary diagram point to moderate to intense weathering in the source region.

The La/Sc, Th/Sc, and La/Co ratios are more enriched and the Cr/Th and Eu/Eu* ratios are more depleted in MF shales than in the PF and HF shales, indicating derivation from a more felsic source than the PF and HF shales. Similarly, the average Zr content in MF shales (475 ± 185) is higher than in PF (133.9 ± 9.3) and HF shales (139.6 ± 18.2), which suggests a more enriched concentration of zircon mineral among the MF than the other shales (F_{calc} = 32.9820669 and $(F_{crit})_{99\%}$ = 6.48949, where $F_{calc} > (F_{crit})_{99\%}$ indicates that data populations are significantly different at 99% confidence level). The LREE enrichment, flat HREE, and negative Eu anomalies in chondrite-normalized plots are attributed to felsic source rock characteristics for the three groups of shales. The trace element concentrations point to an extensional setting (passive margin) for the Jurassic shales (PF and HF) and an active margin setting for the Cretaceous shales (MF).

Key words: Major elements, trace elements, rare earth elements; Huayacocotla anticlinorium, Pimienta Formation, Méndez Formation, ANOVA.

1. Introduction

The geochemistry of shales, especially trace elements, is believed to represent the average composition of the upper continental crust than other sedimentary rocks (DaPeng et al., 2012), since they preserve the original signature of the provenance and diagenetic history (Baioumy and Ismael, 2010; Spalletti et al., 2012; Mondal et al., 2012). In fact, the geochemical composition of clastic sediments is a complex function of variables such as source material, weathering, physical sorting, and diagenesis (Nagarajan et al., 2007a, b; Armstrong-Altrin et al., 2004, 2012; Moosavirad et al., 2012). However, many studies have utilized the geochemical composition of clastic sediments and successfully inferred the source-area weathering conditions (Selvaraj and Chen, 2006; Raza et al., 2012), the provenance (Cullers, 2000, 2002; Armstrong-Altrin, 2009; Bakkiaraj et al., 2010) and the tectonic setting of a sedimentary basin (Armstrong-Altrin and Verma, 2005; Fatima and Khan, 2012). Similarly, the REE patterns and certain trace element ratios of clastic sediments are believed to be an effective tool for the reconstruction of source rock composition because they are not significantly redistributed in the course of sedimentation, lithogenesis, and metamorphism (Basu et al., 1982; Etemad-Saeed et al., 2011; Fu et al., 2010; Zaid, 2012).

This study focuses on the Jurassic (Huayacocotla and Pimienta Formations) and upper Cretaceous (Méndez Formation) shales from the Molango Region, Hidalgo, Mexico. In this article, we discuss the mineralogy, major, and trace element geochemistry of the Mesozoic shales of Mexico. The goal of this study is to constrain the provenance of the shales, which belong to two different periods of the Mesozoic Era and to understand the weathering conditions and tectonic setting of the source region.

2. Geological Setting

The Molango region is located in the northern part of the Hidalgo State, Mexico (Fig. 1). The general stratigraphy of the study area is shown in Table 1 (Morán-Zenteno, 1994). Structurally, the Molango region belongs to the middle portion of the Huayacocotla Anticlinorium, which forms part of the Sierra Madre Oriental (Campa and Coney, 1983; Ochoa-Camarillo et al., 1999).

For the present study, shale samples of the Pimienta (upper Jurassic), Huayacocotla (lower Jurassic), and Méndez (upper Cretaceous) Formations were collected from the localities at El Crucero (Lat. 21°30′02″ N; Long. 98°38′08″ W), Linda Vista (Lat. 20°33′45″ N; Long. 98°30′02″ W), and near Ilamatlán (Lat. 20°46′13″ N; Long. 98°26′42″ W), respectively (Fig. 2).

2.1 Pimienta Formation

The upper Jurassic Pimienta Formation is conformably overlain by the Tamulipas inferior Formation of the lower Cretaceous age (Table 1; Heim, 1926). The rocks are composed of shales, argillaceous limestones, and thin-bedded lime mudstone with chert layers. Thickness of the formation is about 300 m, but it varies due to tectonic thinning or thickening (Suter, 1980).

2.2 Huayacocotla Formation

The Huayacocotla Formation consists of marine deposits containing ammonites of early Jurassic age. The age was assigned based on the *Vermiceras*, *Arnioceras*, *Coroniceras*, *Echioceras*, and *Microderoceras* ammonite fossils (Silva-Pineda and Buitrón-Sánchez, 1999). During the beginning of the Jurassic, continental deposition continued in this part of Mexico with red bed sedimentation, except in the region of the Huayacocotla anticlinorium, where an advance of the seas that induced marine sedimentation of an argillaceous and sandy sequence is recorded. Carrillo-Bravo (1971) termed this Huayacocotla area as "Liassic Basin of Huayacocotla" and named these sedimentary strata as the Huayacocotla Formation, which was deformed at the end of the early Jurassic leading to the predominance of continental deposition in the region during the Middle Jurassic (Morán-Zenteno, 1994).

123 *2.3 Méndez Formation*

124 The upper Cretaceous Méndez Formation (Gamper, 1977) is conformably
125 underlain by the San Felipe Formation (Table 1). This formation consists of yellow-
126 brown argillaceous limestone, intercalated with shale and sandstone. Outcrops are few
127 and the samples of this study are collected at the road-cutting section near to the village
128 Ilamatlán (Fig. 2).

129

130 *2.4 Tectonic setting of the study area*

131 The study area is surrounded towards the South by the Miocene to Recent
132 Mexican Volcanic Belt of a controversial origin, presumably related to extensional
133 tectonics (e.g., Verma, 2002, 2009), towards the West by the Basin and Range province
134 (Suter and Contreras, 2002) and towards the East by the Oligocene to Recent Eastern
135 Alkaline Province (EAP), both of them related to extensional processes (Robin and
136 Tournon, 1978; Luhr et al., 1995; Cruz-Huicochea and Verma, 2013). Cruz-Huicochea
137 and Verma (2013), in fact, used multi-dimensional tectonomagmatic diagrams (Verma et
138 al., 2006; Agrawal et al., 2008; Verma and Agrawal, 2011) to infer the tectonic setting of
139 EAP as a continental rift.

140 During the Lower and Middle Jurassic periods, an extensional event (gravity
141 faulting) produced several tectonic horsts and grabens (Ochoa-Camarillo et al., 1998).
142 The formation of tectonic horsts and grabens continued to the end of the middle Jurassic
143 (Cahuasas red beds). Afterwards, from the late Cretaceous to the late Eocene, the Jurassic
144 and Cretaceous sedimentary rocks were folded, which is called as the laramide Orogeny.

145 This tectonic event produced a complex set of folds and overthrusts called the
146 Huayacocotla anticlinorium. In the final stage, a post-Pliocene extension produced a
147 tectonic valley by normal faulting, which is called as the Molango Graben (Ochoa-
148 Camarillo et al., 1998).

149 The oldest rocks exposed in the Molango region are Precambrian ortho and
150 paragneisses (the Huiznopala gneiss), with protolith magmatic ages between 1200 and
151 1150 Ma (Lawlor et al., 1999). These gneisses are equivalent to the Novillo gneiss
152 (Ciudad Victoria) and to the Oaxaca Complex (Oaxaca) (Ortega-Gutiérrez et al., 1995;
153 Lawlor et al., 1999; Rosales-Lagarde et al., 2005). The Paleozoic rocks exposed along the
154 Huayacocotla area are the Permian Tuzancoa Formation (Guaycamas Formation; Table
155 1).

156

157 **3. Analytical methods**

158

159 Thirty fresh shale samples (Pimienta Formation = 10; Huayacocotla Formation =
160 10; Méndez Formation = 10) were collected from outcrops exposed along the road-cuts
161 (from villages El Crucero, Lindavista, and near Ilamatlán, respectively; Fig. 2). The
162 samples were cleaned in distilled water, dried, and then powdered. By a standard
163 technique, fifteen thin-sections were prepared. Friedman's (1959) organic stain specific
164 for calcite and Katz and Friedman's (1965) combined organic and inorganic stain specific
165 for iron rich calcite have been adopted to identify the mineralogical variations.

166 The mineralogy was studied using the Siemens D5000 X-ray diffractometer
167 (XRD) at the XRF Laboratory, Institute of Geology, Universidad Nacional Autónoma de
168 México (UNAM). About 21 shale samples (7 samples from each formation) were
169 selected for the scanning electron microscopic analysis (SEM) at the Petrology
170 Laboratory, Institute of Geophysics, UNAM. The study was undertaken on a PHILLIPS
171 XL-30 scanning electron microscope (SEM) with a 3.5 nm of resolution. The SEM
172 instrument was equipped with EDAX spectrometer (EDS) system, to determine the
173 chemical composition during SEM observations.

174 The samples were analyzed for major and trace elements. Major elements were
175 analyzed using conventional XRF procedures at the Institute of Geology, UNAM.
176 Powdered samples were heated to 110 degrees C for 6 hours followed by heating in a
177 muffle furnace at 1000°C for two hours to determine LOI (loss on ignition). Lithium
178 tetraborate was mixed with the powdered samples and heated to 1000 degrees C to form
179 a fused sample for X-ray fluorescence analyses. Final analyses were carried out using a
180 Rigaku model RIX-3000 equipped with a Rh tube. Calibration curves were prepared
181 using International reference materials (Lozano-Santa Cruz et al., 1995; Lozano and
182 Bernal, 2005). Resulting chemical analyses for major elements have precisions better
183 than 5%. Major-element data were recalculated to an anhydrous (LOI-free) basis and
184 adjusted to 100% before using them in various diagrams.

185 The trace elements were analyzed at the Korea Basic Science Institute, Daejeon,
186 Korea. Trace element (Ba, Co, Cr, Cu, Ni, Sc, Sr, V, Zn, and Zr) concentrations were
187 determined using a Jobin Yvon 138 Ultrace inductively coupled plasma atomic emission

188 spectrometer (ICP-AES). The REE, Cs, Hf, Nb, Pb, Rb, Th, U, and Y were analyzed by a
189 VG Elemental PQII Plus inductively coupled plasma mass spectrometer (ICP-MS) using
190 a method given by Jarvis (1988). The analytical precision for trace elements is better than
191 5%. The United States Geological Survey Standard MAG-1 was used for calibration.
192 Three analyses were made for each sample and averaged.

193 The statistical information (Tables 2, 3, and 4) was obtained using the
194 DODESSYS software (Verma and Díaz-González, 2012) after the application of all
195 single outlier discordancy tests at 99% confidence level (Verma, 1997; Verma et al.,
196 2009) based on the new precise and accurate critical values (Verma et al., 2008; Verma
197 and Quiroz-Ruiz, 2008, 2011). Only the rounded data are reported following the flexible
198 rules summarized by Verma (2005); such flexible rules are chosen to enable other
199 researchers to apply significance tests (Cruz-Huicochea and Verma, 2013; Verma and
200 Cruz-Huicochea, 2013). Note that the significance tests of Fisher F, Student t and
201 ANOVA require that the data be drawn from normal populations without any statistical
202 contamination. The discordant values not used in the statistical calculations are identified
203 by an asterisk (*). Using an unpublished software UDASYS (by S.P. Verma, R. Cruz-
204 Huicochea, and L. Díaz-González), we applied the ANOVA (Analysis Of Variance) test
205 at 99% confidence level for the compositional data to identify statistically the similarities
206 among the PF, HF, and MF shales. This software uses highly precise and accurate critical
207 values of F (Cruz-Huicochea and Verma, 2013) and t (Verma and Cruz-Huicochea,
208 2013) for the application of significance tests (F, t, and ANOVA). The results are shown
209 in Table 5.

For interpreting the geochemical data of the study area, a database for source rock geochemistry (older rocks) was constructed from the published literature (see Figure 1 for locations and references).

4. Results

4.1. Petrography

4.1.1. Pimienta Formation (PF; upper Jurassic): Siltstone (Fig. 3a) mainly consists of silt-size, angular to subangular quartz and feldspar grains. Monocrystalline quartz with undulatory extinction is the dominant constituent of this petrographic type. Few grains show point and long contacts. The siltstone exhibits both k-feldspar and plagioclase grains. The pore spaces are filled with brown color materials, which indicate the prevalence of iron oxide cementation in this petrographic type.

4.1.2. Huayacocotla Formation (HF; upper Jurassic): Argillaceous siltstone (Fig. 3b) mainly consists of silt grade angular quartz and feldspar grains. Framework grains are showing point and long contacts. Few subrounded grains are also noticed. Some grains are floating in the matriz. Matrix also contains microgranular quartz particles. Monocrystalline quartz with wavy extinction is identified. Polycrystalline quartz is present in minor amount, which displays straight internal boundaries.

4.1.3. Méndez Formation (MF; lower Cretaceous): Laminated ferruginous siltstone (Fig. 3c) exhibits various layers. The lower part is rich in fine-grained quartz and the size of

these grains gradually decreased to silt grade towards the upper part of the thin section, which reveals the fining upward grading. The dark layer seen in the upper part of the photomicrograph is mainly composed of clay-sized materials. The pore spaces are filled with ferruginous materials.

4.2. Mineralogy

The XRD study shows that the PF, HF, and MF shales consist mainly of illite and muscovite clay minerals with little quartz (Fig. 4a, b, and c). A magnetite mineral is identified in the sample EC7 from PF shale (Fig. 4a). The chemical composition measured using SEM-EDS method (qualitative analysis) reveals that the PF and HF shales are rich in phosphate minerals, probably monazite (Fig. 5a), xenotime (Fig. 5b) and/or apatite. A sample (IM10) with high content of Zr is identified in the MF shale (Fig. 5c), which may be a zircon mineral. Slight elevation in potash content is observed in the sample IM5 (Fig. 5d, MF shale).

4.3. Major element geochemistry

Major element concentrations of shales are presented in Table 2. The SiO_2 content is higher in the Méndez Formation (MF) (~ 70.60 - 89.91 wt.%; the mean with one-standard-deviation value being 76.1 ± 6.8; number of samples n = 10), than in the Huayacocotla (HF) (58.90 - 78.00 wt.%; 66.8 ± 6.3; n = 10) and in the Pimienta Formations (PF) (58.70 to 67.70 wt.%; 62.71 ± 2.71; n = 10). The application of ANOVA (Analysis Of Variance) at 99 % confidence level reveals a significant difference in SiO_2

content among the three formations (F_{calc} = 17.40542 and $(F_{crit})_{99\%}$ = 6.48949, where F_{calc} > $(F_{crit})_{99\%}$ indicates that data populations are significantly different at 99% confidence level; Table 5). As expected, the Al_2O_3 content is greater in PF and HF than in MF shales (Table 5), as a result of the dilution effect of quartz (Cullers, 2000). The average K_2O and Na_2O contents are almost similar among the PF, HF, and MF shales (Table 5). The MF shales are lower in Fe_2O_3 (~ 0.23 - 2.22 wt.%) and MgO (~ 0.252 - 0.536 wt.%) contents than in PF (Fe_2O_3 = ~ 5.10 - 8.50 wt.%; MgO ~ 0.90 - 1.20 wt.%) and HF (Fe_2O_3 = 3.30 - 6.10 wt.%; MgO = 0.70 - 1.10 wt.%) shales. There is no statistically significant difference among the PF, HF, and MF shales in P_2O_5 content (F_{calc} = 4.18180 and $(F_{crit})_{99\%}$ = 6.48949, where F_{calc} < $(F_{crit})_{99\%}$ indicates that the data populations are not significantly different at 99% confidence level; Table 5).

On the Fe_2O_3/K_2O vs. SiO_2/Al_2O_3 chemical classification diagram (Fig. 6; Herron, 1988), the MF shales plot in the wacke, arkose, and sub-arkose fields and PF and HF shales mostly plot in the shale field. The MF shales, which plot in the arkose and sub-arkose fields is probably due to high K_2O (samples IM4 and IM 5) and low Fe_2O_3 (IM9 and IM10) contents, respectively, compared to other MF shale samples (Table 2).

4.4. Trace element geochemistry

The trace elements (REE) data are provided in Table 3. The upper Cretaceous MF shales are lower in large ion lithophile elements (LILE; Rb, Cs, Ba, and Sr) and transition

trace elements (TTE; Cr, Co, Ni, V, Sc, and Cu) than in PF and HF (Fig. 7a, b, and c; Table 5) shales. In comparison to upper continental crust (UCC; Taylor and McLennan, 1985), PF and HF shales show smaller variations in trace element concentrations than the MF shales. Except for Sr, Zr, and Hf, the rest of the trace elements in the PF shales have similar composition to the UCC. In the case of HF shales, Sr is depleted and other TTE like V and Co are showing wide variation. Compared to UCC, the MF shales are enriched in Y, Zr, Nb, and Hf (Fig. 7).

Other trace elements like Rb, Ba, Th, and Sr are positively correlated with Al_2O_3 in the PF (linear correlation coefficient r = 0.95, 0.91, 0.87 and 0.54, respectively; n = 10) and HF shales (r = 0.91, 0.99, 0.90, and 0.85; n = 10), indicating that these elements are likely fixed in K-feldspars and clays. On the other hand, the correlation of Al_2O_3 versus Rb, Ba, Th, and Sr is very low or negative for the MF shales (r = 0.47, 0.10, 0.17, -0.51, respectively; n = 10). Similarly, Al_2O_3 is correlated negatively with HFSE like Zr, Hf, and Nb in the MF shales (r = -0.18, -0.17, and -0.22, respectively; n = 10). This reveals that in the MF shales the HFSE are not likely bound in the clay minerals. The concentrations of the TTE (e.g., Cr, Ni, and V) are show a strong correlation with Al_2O_3 for the PF (r = 0.84, 0.73, and 0.70, respectively; n = 10) and HF shales (r = 0.96, 0.39, and 0.92, respectively; n = 10). This relationship suggests that the TTE are fixed in clay minerals. On the other hand, in MF shales the concentration of Al_2O_3 is negatively or poorly correlated with Cr (r = -0.57, n = 10), Ni (r = -0.65, n = 10), and V (r = 0.14, n = 10), indicating that the TTE are not likely fixed in the clay minerals. These variations

may suggest more influx of detrital sediments into the depositional basin during the deposition of the upper Cretaceous MF shales.

4.5. Rare earth element geochemistry

The rare earth elements (REE) data are given in Table 4, and the chondrite normalized patterns (Taylor and McLennan, 1985) are given in Figure 8. The average total REE (∑REE) contents are similar among the PF (178.7 ± 35.0), HF (187.6 ± 34.0), and MF (160 ± 68) shales (F_{calc} = 0.6441114 and $(F_{crit})_{99\%}$ = 4.37800, where $F_{calc} < (F_{crit})_{99\%}$ indicates that data populations are not significantly different at 99% confidence level; Table 5). Two of the MF shales contain higher SiO_2 content (IM9 = 89; IM10 = 91) than the rest of the MF shales, consequently their REE compositions are low (IM9 = 41; IM10 = 63; Table 4). This could be attributed to a dilution effect of quartz (Cullers, 2000).

In general, chondrite normalized REE patterns of the Jurassic PF and HF shales (Fig. 8a and b) are characterized by enriched LREE (La_{CN}/Sm_{CN} = 3.23 and 3.29, respectively; the subscript $_{CN}$ refers to chondrite-normalized values), relatively flat HREE (Gd_{CN}/Yb_{CN} = 1.99 and 1.75, respectively), and negative Eu anomalies (Eu/Eu^* = 0.632 and 0.622, respectively). On the other hand, the LREE fractionation in MF shales (La_{CN}/Sm_{CN}) range from ~ 3.44 - 17.27, but the HREE fractionation (Gd_{CN}/Yb_{CN}) ranges from ~ 0.24 - 1.88. The MF shales have large negative europium anomalies (Eu/Eu^* = 0.298 ± 0.240) (Fig. 8c). Similarly, the chondrite normalized REE patterns of the individual samples from the upper Cretaceous MF shales are not parallel to each other

(Fig. 8c), probably indicating variation in the input of detrital sediments during deposition.

5. Discussion

5.1. Weathering and sediment recycling

The intensity and duration of weathering in clastic sediments can also be evaluated by examining the relationship between alkali and alkaline earth elements (Nesbitt and Young, 1982). The chemical index of alteration is one of the most widely used index [CIA = $(Al_2O_3/Al_2O_3 + CaO^* + Na_2O + K_2O) \times 100$, using molecular proportions] with higher values suggesting more intense chemical weathering (Fadipe et al., 2011; Jayaprakash et al., 2012; Srivastava et al., 2012; Újvári et al., 2012). The CaO^* represents CaO from the silicate fraction. The CaO content in the shales of this study is very low (~ 0.01 - 2.03; Tables 2), hence, the available CaO has been used for the calculation (McLennan et al., 1993). In general, the CIA value for kaolinite and chlorite is nearly 100, while it varies from 70 to 75 for average shale (Nesbitt and Young, 1982). The CIA values in the studied shales vary from ~ 59 to 93 (Table 2). The difference in the average CIA values among PF (71 ± 3), HF (76 ± 6), and MF (73 ± 11) shales is statistically not significant (F_{calc} = 0.7398343 and $(F_{crit})_{99\%}$ = 6.48949, where $F_{calc} < (F_{crit})_{99\%}$ indicates that data populations are not significantly different at 99% confidence level; Table 5) and are within the range of PAAS values (70-75; Taylor and McLennan, 1985). These values indicate a moderate to intense chemical weathering in the source

area. The MF shales have a wide range in CIA values (~ 59 - 93; Table 2), indicating the combination of both mature and immature sediments, which is consistent with the dispersion observed in the SiO_2/Al_2O_3 ratios (Fig. 6).

The CIA values are also plotted in Al_2O_3 - (CaO^* + Na_2O) - K_2O (A-CN-K) triangular diagram (molecular proportion; Fedo et al., 1996; Fig. 9) which identifies the differentiation of compositional changes associated with chemical weathering and/or source rock composition (e.g., Ghosh et al., 2012). In the Figure 9, individual samples plot away from the plagioclase-K-feldspar join line, indicating moderate to intense chemical weathering in the source area. The PF shales are parallel to the A-CN line, showing the leaching of CaO and Na_2O under moderate to intensive weathering processes from source rocks of the upper continental crust, e.g., granodiorite and granite. Samples plotting significantly off the predicted weathering trend (trend 1) and towards the K_2O apex (trend 2) are interpreted to have likely been affected by potassium metasomatism (e.g., four MF shales), which involves post depositional conversion of kaolin to illite (Fedo et al., 1995). This conversion process produces K_2O enrichment and results in lowering of CIA values. This can be corrected by simply projecting a line from the K-apex through a given data, meet until the predicted weathering trend is intersected (trend 1), which gives the premetasomatized CIA value (Fedo et al., 1995). For example, the calculated CIA values of two MF shale samples IM4 and IM5 are 59.30 and 59.11, respectively (Table 2) and their premetasomatized values are predicted to be 68.30 and 68.11, respectively (Fig. 9). Thus, the premetasomatized values of MF shales (four samples) fall in a narrow range and close to the PF and HF shales.

Nesbitt et al. (1997) illustrated that the CIA values may also be influenced by tectonism. In the present study, for MF shales, the degree of weathering is non-uniform and quite variable (~ 67 - 93; Table 2). This spread of CIA values in MF shales is typical of non-steady state weathering conditions, which probably indicates active tectonism or rapid uplift during the upper Cretaceous.

McLennan et al. (1993) observed that the Th/Sc ratio is a sensitive index of the bulk composition of the provenance, and the Zr/Sc ratio is a useful index of zircon enrichment. Thus, the Th/Sc vs. Zr/Sc bivariate plot can be used to discriminate the compositional variation, the degree of sediment recycling, and heavy mineral sorting (e.g., Yan et al., 2012; Long et al., 2012). On the Th/Sc-Zr/Sc diagram (Fig. 10), the shales display two compositional trends with most samples gathered near average UCC composition (trend 1), which is indicative of a minimal influence of mineral sorting. Samples plotting along trend 2 are indicative of concentration of zircon by sediment recycling and sorting. The Zr/Sc ratios for the PF (~ 7.17 - 10.53) and HF (~ 6.94 - 20.57) shales are significantly lower than for the MF (~ 50 - 316) shales, suggesting a higher concentration of zircon in the latter (F_{calc} = 35.0858032 and $(F_{crit})_{99\%}$ = 6.48949, where $F_{calc} > (F_{crit})_{99\%}$ indicates that data populations are significantly different at 99% confidence level; Table 5). This fact is also supported by the larger variation of Zr/Al_2O_3 ratio in MF (~ 10 - 100) shales than in the HF (~ 6 - 15) and PF (~ 6 - 9) shales (F_{calc} = 15.85075 and $(F_{crit})_{99\%}$ = 6.48949, where $F_{calc} > (F_{crit})_{99\%}$ indicates that data populations are significantly different at 99% confidence level; Table 5). The enrichment of Zr content, especially in the MF shales could be due to the concentration of zircon mineral.

383 This observation is consistent with the results obtained by the SEM-EDS method (Fig.
384 5c). Lawlor et al. (1999) and Lopez et al. (2001) also reported the abundance of equant
385 and elongated zircon grains in gneisses (Huiznopala area) and granites (Las Delicias
386 Formation) exposed relatively near to the study area (Fig. 1).
387
388 *5.2 Provenance*
389 The geochemistry of clastic sediments has been widely used to identify the
390 provenance (Cullers, 1995; Armstrong-Altrin et al., 2004, 2012; Jafarzadeh and Hosseini-
391 Barzi, 2008; Baioumy and Ismael, 2010). The Zr concentration in clastic sediments can
392 be used to characterize the nature and composition of source rocks (e.g., Run-sheng et al.,
393 2012). The average Zr concentration in MF shales (475 ± 185) is higher than in PF (133.9
394 ± 9.3) and HF shales (139.6 ± 18.2) (F_{calc} = 32.9820669 and $(F_{crit})_{99\%}$ = 6.48949, where
395 $F_{calc} > (F_{crit})_{99\%}$ indicates that data populations are significantly different at 99%
396 confidence level; Table 5). The MF shales show a low positive correlation between Zr
397 and HREE (r = 0.45), whereas correlation is absent in PF (r = -0.10) and HF (r = -0.09)
398 shales. This suggests that the concentration of zircon has no influence on the HREE in PF
399 and HF shales, although there may be some on MF shales.
400 In addition, ∑REE is positively correlated with K_2O in PF (r = 0.98) and HF (r =
401 0.99) shales, but the correlation is poor in MF (r = 0.23) shales, suggesting that illite may
402 be the host of REE in the PF and HF shales. The XRD data is consistent with this
403 observation (Fig. 4). There is also a positive correlation between ∑REE and P_2O_5 in PF (r
404 = 0.90) shales. This correlation, however, is poor for HF (= 0.31) and MF (r = 0.15)

shales. This indicates that phosphate rich minerals such as apatite and/or xenotime may control the REE abundances in the PF shales. The SEM-EDS study also reveals a phosphate rich composition for the PF and HF shales (Fig. 5).

The Eu/Eu^{*}, $(La/Lu)_{cn}$, La/Sc, La/Co, Th/Sc, Th/Co, and Cr/Th are widely used to understand the provenance composition of the source region since REE, Th, and La abundances are higher in felsic rocks than in basic rocks, whereas, the Co, Sc and Cr contents are higher in mafic rocks than in felsic rocks (Cullers, 1994, 2000, 2002; Armstrong-Altrin et al., 2004; Osae, et al., 2006; Armstrong-Altrin, 2009; Tijani et al., 2010). These ratios are compared in Table 6 with those of possible source rocks, the UCC, and from sediment derived from mafic and felsic rocks. In this study, the Eu/Eu^{*}, $(La/Lu)_{CN}$, La/Sc, La/Co, Th/Sc, Th/Co, and Cr/Th ratios of the PF and HF shales fall within the range of sediments derived from felsic source rocks. In addition, elevated concentrations of Cr (> 150) and Ni (> 100) and low Cr/Ni ratios (between 1.3 and 1.5) are indicative of some ultramafic rocks in the source (Garver et al., 1996). The PF, HF, and MF shales have low average Cr (116, 108, and 20 ppm, respectively), Ni (48, 45, and 5 ppm, respectively), and high Cr/Ni (~ 2.1-3.3, ~ 1.5-3.6, and ~ 3.5-5.6, respectively) ratios. The low Cr and Ni values and the high Cr/Ni ratio, indicate the absence of ultramafic detritus in the provenance (Table 3).

The REE patterns and the size of the Eu anomalies in sediments also provide important clues on source rock characteristics. Higher LREE/HREE ratios and negative Eu anomalies are the characteristics of felsic source rocks, whereas lower LREE/HREE ratios and little and absence of Eu anomalies are characteristic of mafic rocks (Cullers,

427 1994). In the present study, the high LREE/HREE ratios and significant negative Eu
428 anomalies are attributed to felsic source rock characteristics for the PF, HF, and MF
429 shales (Fig. 8a-c). Taylor and McLennan (1985) observed that the granitic rocks formed
430 during Phanerozoic Eon have more K-feldspar rich granites and thereby reflect less
431 depletion of Eu, and high depletion of HREE with $(Gd/Yb)_{CN}$ ratio < 2. On the Eu/Eu^* vs
432 $(Gd/Yb)_{cn}$ plot (Fig. 11), except two samples, the remaining samples plot in the post-
433 Archean field with $(Gd/Yb)_{cn}$ = 0.24-1.98. The average REE data of the gneisses
434 (Proterozoic Huiznopala gneiss; Lawlor et al., 1999) and granites (conglomerate-bearing
435 layer of the late Paleozoic Las Delicias Formation, exposed near Las Uvas, Coahuila,
436 northeastern Mexico; Lopez et al., 2001), located relatively near to the study area (refer
437 Fig. 1 for locations) are also shown in this diagram (Fig. 11). The shales of this study,
438 plot close to the average granite (Lopez et al., 2001) from the late Paleozoic Las Delicias
439 Formation (Fig. 1). This diagram further illustrates the larger negative Eu anomalies in
440 the MF shales (Eu/Eu^* = 0.13-0.76) compared to the PF (Eu/Eu^* = 0.59-0.67) and HF
441 (Eu/Eu^* = 0.60-0.65) shales (Table 4). The large negative Eu anomaly in the MF shales is
442 most probably due to the depletion of plagioclase. The ANOVA test at 99% confidence
443 level for ∑REE content demonstrates that the studied shales are compositionally similar
444 to the gneiss (Lawlor et al., 1999) and granite (Lopez et al., 2001) rocks, exposed
445 relatively close to the study area (F_{calc} = 0.64411 and $(F_{crit})_{99\%}$ = 4.37800, where F_{calc} <
446 $(F_{crit})_{99\%}$ indicates that data populations are not significantly different at 99% confidence
447 level; Table 5).

448 Lopez et al. (2001) stated that the isotopic studies and U-Pb dating of zircons
449 from Precambrian granitoids that occur as cobbles and boulders in the Paleozoic
450 conglomerate exposed in the state of Coahuila have Grenvillian crystallization ages from
451 1232 ± 7 to 1214 ± 2 Ma. Therefore, based on Lopez et al. (2001), the present study
452 provides a clue that the detritus of the Delicias Formation and shales of the Molango
453 region were possibly derived from a similar source.
454
455 *5.3. Tectonic Setting*
456 Tectonic setting discrimination diagrams proposed by Bhatia (1983) and Roser
457 and Korsch (1986) have been extensively used in sedimentary geochemistry to identify
458 the tectonic setting of unknown sedimentary basins (e.g., Purevjav and Roser, 2012; Yan
459 et al., 2012). However, in recent years tectonic discrimination based on major elements
460 has received considerable criticism (Armstrong-Altrin and Verma, 2005; Ryan and
461 Williams, 2007), whereas schemes that depend on trace elements have been considered as
462 relatively reliable (LaMaskin et al., 2008). Most conventional bivariate and ternary
463 tectonic discrimination diagrams are plagued by the incorrect statistical data handling
464 (see, e.g. Agrawal and Verma, 2007; Verma, 2010). Nevertheless, instead of using major
465 element based diagrams, the trace elements discrimination diagram of Bhatia and Crook
466 (1986) is used to infer the tectonic setting. On the Sc/Cr-La/Y diagram (Fig. 12) most of
467 the studied shale samples plot in the passive margin field, except few MF shale samples,
468 which fall in the continental island arc field with scatter.

The tectonic environments can also be inferred based on the REE distribution in clastic sediments (Bhatia, 1985; McLennan and Taylor, 1991; McLennan et al., 1993). Bhatia (1985) documented that passive margin is typically characterized by uniform REE patterns similar to PAAS (Post Archaean Average Australian Shale) with pronounced negative Eu anomaly, while sediments from active continental margin display fractionated REE patterns with wide range of negative Eu anomaly. In the present study, the PF and HF shales shows relatively similar REE patterns, with pronounced negative Eu anomalies (Eu/Eu^{*} = ~ 0.59-0.66), which favour for the passive margin, probably suggesting an extensional event during the Jurassic. On the other hand, fractionated REE patterns (ΣREE = ~ 41-237) and wide range in Eu anomaly (Eu/Eu^{*} = ~ 0.130-0.762) of the MF shale samples may suggest an active tectonism, probably an uplift, during the upper Cretaceous (Table 4). However, further research is needed to infer exactly the tectonic setting of the study area.

6. Conclusion

The chemical index of alteration (CIA) values of the studied shale samples indicate that the intensity of chemical weathering in the source area was probably moderate to intense. The Eu/Eu^{*}, $(La/Lu)_{cn}$, La/Sc, La/Co, Th/Sc, Th/Co, and Cr/Th ratios reveal that the shales were derived from mostly felsic source rocks. The low Cr and Ni contents and high Cr/Ni ratio suggest an absence of ultramafic components in the provenance. The chondrite normalized REE patterns of the shales are characterized by

enriched LREE, relatively flat HREE, and negative Eu anomalies. The large negative Eu anomalies, high Zr, Hf contents and Zr/Al_2O_3 ratio in the MF shales indicate a more felsic nature than the HF and PF shales. The compositional similarity among the three formations (PF, HF, and MF) is tested statistically by the application of ANOVA (Analysis Of Variance) at 99% confidence level to avoid misinterpretation.

The present study provides a clue that the detritus of the Delicias Formation and shales of the Molango region were possibly derived from a similar source. The trace element concentrations of PF and HF shale samples suggest a passive margin setting, probably indicating an extensional event occurred during the Jurassic. A wide spread of CIA values and highly fractionated REE pattern in MF shales may suggest the unstable tectonic regime with little mixing of sediment during the deposition of the upper Cretaceous MF shales.

Acknowledgement

This work is part of the BSc thesis completed by the co-authors Adriana Cruz-Martinez and Gladis Avila-Ramirez. We express our gratitude to the laboratory technicians Eduardo Morales de la Garza, Susana Santiago-Perez, Héctor M. Alexander-Valdés, and Ricardo Martinez for their invaluable assistance. We thank the staffs Patricia Girón García for XRD analysis and Carlos Linares-López for SEM-EDS study, which helped to revise the manuscript within time. The authors are grateful to Elisa Liliana Hidalgo and Olmedo Natalhy-Pineda for the assistance during SEM-EDS study. Rufino

514 Lozano SantaCruz, geochemist, Institute of Geology, UNAM (Universidad Nacional
515 Autónoma de México), is greatly thanked for chemical analysis. Special appreciation
516 goes to Lic. Arturo Ferrer Méndez Flores, librarian, UNAM for providing the geology
517 map. We are grateful to the reviewers Peter Stille and Robert L. Cullers and Associate
518 Editor François Chabaux for numerous helpful comments to improve our paper. Yong Il
519 Lee is grateful for the financial support from the Korea Research Foundation (grant no.
520 2010-0009765). This research was supported financially by the Instituto de Ciencias del
521 Mar y Limnología, Universidad Nacional Autónoma de México, Institutional (No. 616)
522 and PAPIIT (IA101213) Projects.
523
524
525
526
527
528
529
530
531
532
533
534
535

References

Agrawal, S., Verma, S.P., 2007. Comment on "Tectonic classification of basalts with classification trees" by Pieter Vermeesch (2006). Geochimica et Cosmochimica Acta 71, 3388-3390.

Agrawal, S., Guevara, M., Verma, S.P., 2008. Tectonic discrimination of basic and ultrabasic rocks through log-transformed ratios of immobile trace elements. International Geology Review 50, 1057-1079.

Armstrong-Altrin, J.S., 2009. Provenance of sands from Cazones, Acapulco, and Bahía Kino beaches, Mexíco. Revista Mexicana de Ciencias Geológicas 26(3), 764-782.

Armstrong-Altrin, J.S., Verma, S.P., 2005. Critical evaluation of six tectonic setting discrimination diagrams using geochemical data of Neogene sediments from known tectonic settings. Sedimentary Geology 177, 115-129.

Armstrong-Altrin, J.S., Lee, Y.I., Verma, S.P., Ramasamy, S., 2004. Geochemistry of sandstones from the Upper Miocene Kudankulam Formation, southern India: Implications for provenance, weathering, and tectonic setting. Journal of Sedimentary Research 74, 285-297.

Armstrong-Altrin, J.S., Lee, Y.I., Kasper-Zubillaga, J.J., Carranza-Edwards, A., Garcia, D., Eby, N., Balaram, V., Cruz-Ortiz, N.L., 2012. Geochemistry of beach sands along the western Gulf of Mexico, Mexico: Implication for provenance. Chemie der Erde / Geochemistry 72, 345-362.

557 Baioumy, H.M., Ismael, I.S., 2010. Factors controlling the compositional variations
558 among the marine and non-marine black shales from Egypt. International Journal
559 of Coal Geology 83 (1), 35-45.

560 Bakkiaraj, D., Nagendra, R., Nagarajan, R., Armstrong-Altrin, J.S., 2010. Geochemistry
561 of sandstones from the Upper Cretaceous Sillakkudi Formation, Cauvery Basin,
562 Southern India: Implication for provenance. Journal of the Geological Society of
563 India 76, 453-467.

564 Basu, A., Blanchard, D.P., Brannon, J.C., 1982. Rare earth elements in the sedimentary
565 cycle: a pilot study of the first leg. Sedimentology 29, 737-742.

566 Bhatia, M.R., 1983. Plate tectonics and geochemical composition of sandstones. The
567 Journal of Geology 91, 611-627.

568 Bhatia, M.R., 1985. Rare earth element geochemistry of Australian Paleozoic graywackes
569 and mudrocks: provenance and tectonic control. Sedimentary Geology 45, 97-
570 113.

571 Bhatia, M.R., Crook, K.A.W., 1986. Trace element characteristics of graywackes and
572 tectonic setting discrimination of sedimentary basins. Contributions to Mineralogy
573 and Petrology 92, 181-193.

574 Campa, M.F., Coney, P.J., 1983. Tectono-stratigraphic terranes and mineral resource
575 distributions in Mexico. Canadian Journal of Earth Sciences 20, 1040-1051.

576 Carrillo-Bravo, J., 1971. La Plataforma Valles-San Luis Potosí. Boletín de la Asociación
577 Mexicana de Geólogos Petroleros 23 (1-6), 1-112.

578 Cruz-Huicochea, R., Verma, S.P., 2013. New critical values for F and their use in the
579 ANOVA and Fisher´s F tests for evaluating geochemical data. Journal of Iberian
580 Geology (in press).

581 Condie, K.C., 1993. Chemical composition and evolution of upper continental crust:
582 contrasting results from surface samples and shales. Chemical Geology 104, 1-37.

583 Cullers, R.L., 1994. The controls on the major and trace element variation of shales,
584 siltstones, and sandstones of Pennsylvanian-Permian age from uplifted continental
585 blocks in Colorado to platform sediment in Kansas, USA. Geochimica et
586 Cosmochimica Acta 58, 4955-4972.

587 Cullers, R.L., 1995. The controls on the major and trace element evolution of shales,
588 siltstones and sandstones of Ordovician to Tertiary age in the Wet Mountain
589 region, Colorado, U.S.A. Chemical Geology 123, 107-131.

590 Cullers, R.L., 2000. The geochemistry of shales, siltstones and sandstones of
591 Pennsylvanian - Permian age, Colorado, U.S.A.: Implications for provenance and
592 metamorphic studies. Lithos 51, 181-203.

593 Cullers, R.L., 2002. Implications of elemental concentrations for provenance, redox
594 conditions, and metamorphic studies of shales and limestones near Pueblo, CO,
595 USA. Chemical Geology 191, 305-327.

596 Cullers, R.L., Podkovyrov, V.N., 2000. Geochemistry of the Mesoproterozoic Lakhanda
597 shales in southeastern Yakutia, Russia: implications for mineralogical and
598 provenance control, and recycling. Precambrian Research 104, 77-93.

599 DaPeng, L., YueLong, C., Zhong, W., Yu, L., Jian, Z., 2012. Paleozoic sedimentary
600 record of the Xing-Meng Orogenic Belt, Inner Mongolia: Implications for the
601 provenances and tectonic evolution of the Central Asian Orogenic Belt. Chinese
602 Science Bulletin 57(7), 776-785.

603 Etemad-Saeed, N., Hosseini-Barzi, M., Armstrong-Altrin, J.S., 2011. Petrography and
604 geochemistry of clastic sedimentary rocks as evidence for provenance of the
605 Lower Cambrian Lalun Formation, Posht-e-badam block, Central Iran. Journal of
606 African Earth Sciences 61, 142-159.

607 Fadipe, O.A., Carey, P.F., Akinlua, A., Adekola, S.A., 2011. Provenance, diagenesis and
608 reservoir quality of the lower Cretaceous sandstone of the Orange Basin, South
609 Africa. South African Journal of Geology 114 (3-4), 433-448.

610 Fatima, S., Khan, M.S., 2012. Petrographic and geochemical characteristics of
611 Mesoproterozoic Kumbalgarh clastic rocks, NW Indian shield: implications for
612 provenance, tectonic setting, and crustal evolution. International Geology Review
613 54(10), 1113-1144.

614 Fedo, C.M., Nesbitt, H.W., Young, G.M., 1995. Unraveling the effects of potassium
615 metasomatism in sedimentary rocks and paleosols, with implications for
616 paleoweathering conditions and provenance. Geology 23, 921-924.

617 Fedo, C.M., Eriksson, K., Krogstad, E.J., 1996. Geochemistry of shales from the Archean
618 (~ 3.0 Ga) Buhwa Greenstone Belt, Zimbabwe: Implications for provenance and
619 source-area weathering. Geochimica et Cosmochimica Acta 60, 1751-1763.

620 Friedman, G.M., 1959. Identification of carbonate minerals by staining methods. Journal
621 of Sedimentary Petrology 29, 87-97.

622 Fu, X., Wang, J., Zeng, Y., Tan, F., Feng, X., 2010. REE geochemistry of marine oil
623 shale from the Changshe Mountain area, northern Tibet, China. International
624 Journal of Coal Geology 81, 191-199.

625 Gamper, M.A., 1977. Acerca del límite Cretácico-Terciario en México: Universidad
626 Nacional Autónoma de México, Instituto de Geología, Revista 1, 23-27.

627 Garver, J.I., Royce, P.R., Smick, T.A., 1996. Chromium and nickel in shale of the
628 Taconic Foreland: a case study for the provenance of fine-grained sediments with
629 an ultramafic source. Journal of Sedimentary Research 66, 100-106.

630 Ghosh, S., Sarkar, S., Ghosh, P., 2012. Petrography and major element geochemistry of
631 the Permo-Triassic sandstones, central India: Implications for provenance in an
632 intracratonic pull-apart basin. Journal of Asian Earth Sciences 43, 207-240.

633 Heim, A., 1926. Notes on the Jurassic of Tamazunchale (Sierra Madre Oriental, Mexico):
634 Eclogae Geol. Helvetiae 20, 84-87.

635 Herron, M.M., 1988. Geochemical classification of terrigenous sands and shales from
636 core or log data. Journal of Sedimentary Petrology 58, 820-829.

637 Jafarzadeh, M., Hosseini-Barzi, M., 2008, Petrography and geochemistry of Ahwaz
638 sandstone member of Asmari Formation, Zagros, Iran: implications on
639 provenance and tectonic setting. Revista Mexicana de Ciencias Geológicas 25(2),
640 247-260.

641 Jarvis, K.E., 1988. Inductively coupled plasma mass spectrometry: A new technique for
642 the rapid or ultra level determination of the rare-earth elements in geological
643 materials. Chemical Geology 68, 31-39.

644 Jayaprakash, M., Nagarajan, R., Velmurugan, P.M., Sathiyamoorthy, J., Krishnamurthy,
645 R.R., Urban, B., 2012. Assessment of trace metal contamination in a historical
646 freshwater canal (Buckingham Canal), Chennai, India. Environmental Monitoring
647 and Assessment 184, 7407-7424.

648 Katz, A., Friedman, G.M., 1965. The preparation of stained acetate peels for the study of
649 carbonate rocks. Journal of Sedimentary Petrology 35, 248-249.

650 Keppie, J.D., 2004. Terranes of Mexico Revisited: A 1.3 Billion Year Odyssey:
651 International Geology Review 46, 765-794.

LaMaskin, T.A., Dorsey, R., Vervoort, J.D., 2008. Tectonic controls on mudrock geochemistry, Mesozoic rocks of eastern Oregon and western Idaho, U.S.A.: Implications for Cordilleran tectonics. Journal of Sedimentary Research 78(12), 765-783.

Lawlor, P.J., Ortega-Gutiérrez, F., Cameron, K.L., Ochoa-Camarillo, H., López, R., Sampson, D.E., 1999. U-Pb geochronology, geochemistry, and provenance of the Greenvillian Huiznopala Gneiss of Eastern Mexico. Precambrian Research 94, 73-99.

Long, X., Yuan, C., Sun, M., Xiao, W., Wang, Y., Cai, K., Jiang, Y., 2012. Geochemistry and Nd isotopic composition of the Early Paleozoic flysch sequence in the Chinese Altai, Central Asia: Evidence for a northward-derived mafic source and insight into Nd model ages in accretionary orogen. Gondwana Research 22, 554-566.

Lopez, R.L., Cameron, K.L., Jones, N.W., 2001. Evidence for Paleoproterozoic, Grenvillian, and Pan-African age Gondwanan crust beneath northeastern Mexico. Precambrian Research 107, 195-214.

Lozano, R., Bernal, J.P., 2005. Characterization of a new set of eight geochemical reference materials for XRF major and trace element analysis. Revista Mexicana de Ciencias Geológicas 22 (3), 329-344.

671 Lozano-Santa Cruz, R., Verma, S.P., Girón, P., Velasco, F., Morán Zenteno, D., Viera,
672 F., Chávez, G., 1995. Calibración preliminar de fluorescencia de rayos-X para
673 análisis cuantitativo de elementos mayores en rocas ígneas. Actas INAGEQ 1,
674 203-208.

675 Luhr, J.F., Pier, J.G., Aranda-Gómez, J.J., Podosek, F.A., 1995. Crustal contamination in
676 early Basin-and-Range hawaiites of the Los Encinos volcanic field, central
677 México. Contributions to Mineralogy and Petrology 118, 321-339.

678 McLennan, S.M., Taylor, S.R., 1991. Sedimentary rocks and crustal evolution: tectonic
679 setting and secular trends. Journal of Geology 99, 1-21.

680 McLennan, S.M., Hemming, S., McDaniel, D.K., Hanson, G.N., 1993. Geochemical
681 approaches to sedimentation, provenance, and tectonics, In: Johnsson, M.J., Basu,
682 A. (Eds.), Processes controlling the composition of clastic sediments. Geological
683 Society of America, Special Paper no. 284, pp. 21-40.

684 Moosavirad, S.M., Janardhana, M.R., Sethumadhav, M.S., Narasimha, K.N.P., 2012.
685 Geochemistry of lower Jurassic sandstones of Shemshak Formation, Kerman
686 Basin, Central Iran: Provenance, source weathering and tectonic setting. Journal
687 of the Geological Society of India 79, 483-496.

688 Mondal, M.E.A., Wani, H., Mondal, B., 2012. Geochemical signature of provenance,
689 tectonics and chemical weathering in the Quaternary flood plain sediments of the
690 Hindon River, Gangetic plain, India. Tectonophysics 566-567, 87-94.

691 Morán-Zenteno, D., 1994. The Geology of the Mexican Republic. AAPG studies in
692 Geology, no. 39.

693 Nagarajan, R., Madhavaraju, J., Nagendra, R., Armstrong-Altrin, J.S., Moutte, J., 2007a.
694 Geochemistry of Neoproterozoic shales of Rabanpalli formation, Bhima basin,
695 northern Karnataka, southern India: implications for provenance and paleoredox
696 conditions. Revista Mexicana de Ciencias Geológicas 24(2), 150-160.

697 Nagarajan, R., Armstrong-Altrin, J.S., Nagendra, R., Madhavaraju, J., Moutte, J., 2007b.
698 Petrography and geochemistry of terrigenous sedimentary rocks in the
699 Neoproterozoic Rabanpalli Formation, Bhima Basin, southern India: Implications
700 for paleoweathering condition, provenance, and source rock composition. Journal
701 of the Geological Society of India 70(2), 297-312.

702 Nesbitt, H.W., Young, G.M., 1982. Early Proterozoic climates and plate motions inferred
703 from major element chemistry of lutites. Nature 299, 715-717.

704 Nesbitt, H.W., Fedo, C.M., Young, G.M., 1997. Quartz and feldspar stability, steady and
705 non-steady-state weathering, and petrogenesis of siliciclastic sands and muds.
706 Journal of Geology 105, 173-191.

707 Ochoa-Camarillo, H.R., Buitrón, B.E., Silva-Pineda, A., 1998. Contribución al
708 conocimiento de la bioestratigrafía, paleoecología y tectónica del Jurásico
709 (Anticlinorio de Huayacocotla) en la región de Molango, Hidalgo, México.
710 Revista Mexicana de Ciencias Geológicas 15(1), 57-63.

711 Ochoa-Camarillo, H., Buitrón-Sánchez, B., Silva-Pineda, A., 1999. Red beds of the
712 Huayacocotla Anticlinorium, state of Hidalgo, east-central Mexico, in Bartolini,
713 C., Wilson, J. L., and Lawton, T. F., eds., Mesozoic sedimentary and tectonic
714 history of north-central Mexico: Boulder, Colorado, Geological Society of
715 America Special Paper 340, p. 59-68.

716 Ortega-Gutiérrez, F., Ruiz, J., Centeno-García, E., 1995. Oaxaquia, a Proterozoic
717 microcontinent accreted to North America during the late Paleozoic. Geology 23,
718 1127-1130.

719 Osae, S., Asiedu, D.K., Banoeng-Yakubo, B., Koeberl, C., Dampare, S.B., 2006.
720 Provenance and tectonic setting of Late Proterozoic Buem sandstones of
721 southeastern Ghana: Evidence from geochemistry and detrital modes. Journal of
722 African Earth Sciences 44, 85-96.

723 Purevjav, N., Roser, B., 2012. Geochemistry of Devonian-Carboniferous clastic
724 sediments of the Tsetserleg terrane, Hangay Basin, central Mongolia: Provenance,
725 source weathering, and tectonic setting. Island Arc 21, 270-287.

726 Raza, M., Ahmad, A.H.M., Khan, M.S., Khan, F., 2012. Geochemistry and detrital modes
727 of Proterozoic sedimentary rocks, Bayana Basin, north Delhi fold belt:
728 implications for provenance and source-area weathering. International Geology
729 Review 54(1), 111-129.

730 Robin, C., Tournon, J., 1978. Spatial relations of andesitic and alkaline provinces of
731 Mexico and Central America. Canadian Journal of Earth Sciences 15, 1633-1641.

732 Rosales-Lagarde, L., Centeno-García, E., Dostal, J., Sour-Tovar, F., Ochoa-Camarillo,
733 H., Quiroz-Barroso, S., 2005. The Tuzancoa Formation: Evidence of an Early
734 Permian Submarine Continental Arc in East-Central Mexico. International
735 Geology Review 47 (9), 901-919.

736 Roser, B.P., Korsch, R.J., 1986. Determination of tectonic setting of sandstone-mudstone
737 suites using SiO_2 content and K_2O/Na_2O ratio. Journal of Geology 94(5), 635-
738 650.

739 Run-sheng, H., Cong-Qiang, L., Carranza, E.J.M., Baohong, H., Zhi-Long, H., Xue-Kun,
740 W., Yu-Zhao, H., Li, L., 2012. REE geochemistry of altered tectonites in the
741 Huize base-metal district, Yunnan, China. Geochemistry: Exploration,
742 Environment, Analysis 12, 127-146.

743 Ryan, K.M., Williams, D.M., 2007. Testing the reliability of discrimination diagrams for
744 determining the tectonic depositional environment of ancient sedimentary basins.
745 Chemical Geology 242(1-2), 103-125.

746 Selvaraj, K., Chen, C.-T.A., 2006. Moderate chemical weathering of subtropical Taiwan:
747 Constraints from solid-phase geochemistry of sediments and sedimentary rocks.
748 Journal of Geology 114(1), 101-116.

749 Silva-Pineda, A., Buitrón-Sánchez, B.S., 1999. Mesozoic redbed floras in east-central
750 Mexico and their stratigraphic relationships with marine beds, in Bartolini, C.,
751 Wilson, J. L., and Lawton, T. F., eds., Mesozoic sedimentary and Tectonic
752 History of North-Central Mexico: Boulder, Colorado, Geological Society of
753 America Special Paper 340, p. 151-160.

754 Spalletti, L.A., Limarino, C.O., Piñol, F.C., 2012. Petrology and geochemistry of
755 Carboniferous siliciclastics from the Argentine Frontal Cordillera: A test of
756 methods for interpreting provenance and tectonic Setting. Journal of South
757 American Earth Sciences 36, 32-54.

758 Srivastava, A.K., Randive, K.R., Khare, N., 2012. Mineralogical and geochemical studies
759 of glacial sediments from Schirmacher Oasis, East Antarctica. Quaternary
760 International, http://dx.doi.org/10.1016/j.quaint.2012.07.028.

761 Suter, M., 1980. Tectonics of the external part of the Sierra Madre Oriental foreland
762 thrust-and-fold belt between Xilitla and the Moctezuma river (Hidalgo and San
763 Luis Potosi states). Universidad Nacional Autónoma de México, Instituto de
764 Geología, Revista 4(1), 19-31.

765 Suter, M., Contreras, J., 2002. Active tectonics of northeastern Sonora, Mexico (Southern
766 Basin and Range Province) and the 3 May 1887 M_W 7.4 earthquake. Bulletin of
767 the Seismological Society of America 92(2), 581-589.

768 Taylor, S.R., McLennan, S.M., 1985. The Continental Crust: Its Composition and
769 Evolution. Blackwell, Oxford, UK, pp. 349.

770 Tijani, M.N., Nton, M.E., Kitagawa, R., 2010. Textural and geochemical characteristics
771 of the Ajali Sandstone, Anambra Basin, SE Nigeria: Implication for its
772 provenance. Comptes Rendus Geoscience 342, 136-150.

773 Újvári, G., Varga, A., Raucsik, B., Kovács, J., 2012. The Paks loess-paleosol sequence: A
774 record of chemical weathering and provenance for the last 800 ka in the mid-
775 Carpathian Basin. Quaternary International doi: 10.1016/j.quaint.2012.04.004.

776 Verma, S.P., 1997. Sixteen statistical tests for outlier detection and rejection in evaluation
777 of International Geochemical Reference Materials: Example of micro gabbro PM-
778 S. Geostandards Newsletter The Journal of Geostandards and Geoanalysis 21, 59-
779 75.

780 Verma, S.P., 2002. Absence of Cocos plate subduction-related basic volcanism in
781 southern Mexico: a unique case on Earth?. Geology 30 (12), 1095-1098.

782 Verma, S.P., 2005. Estadística Básica para el Manejo de Datos Experimentales:
783 Aplicación a la Geoquímica (Geoquimiometría). Universidad Nacional Autónoma
784 de México, México, D.F., 186 p. ISBN: 970-32-3000-8.

785 Verma, S.P., 2009. Continental rift setting for the central part of the Mexican Volcanic
786 Belt: A statistical approach. Open Geology Journal 3, 8-29.

787 Verma, S.P., 2010. Statistical evaluation of bivariate, ternary and discriminant function
788 tectonomagmatic discrimination diagrams. Turkish Journal of Earth Sciences 19
789 (2), 185-238.

790 Verma, S.P., Quiroz-Ruiz, A., 2008. Critical values for 33 discordancy test variants for
791 outliers in normal samples for very large sizes of 1,000 to 30,000 and evaluation
792 of different regression models for the interpolation and extrapolation of critical
793 values. Revista Mexicana de Ciencias Geológicas 25, 369-381.

794 Verma, S.P., Agrawal, S., 2011. New tectonic discrimination diagrams for basic and
795 ultrabasic volcanic rocks through log-transformed ratios of high field strength
796 elements and implications for petrogenetic processes. Revista Mexicana de
797 Ciencias Geológicas 28, 24-44.

798 Verma, S.P., Quiroz-Ruiz, A., 2011. Corrigendum to Critical values for 22 discordancy
799 test variants for outliers in normal samples up to sizes 100, and applications in
800 Science and Engineering [Rev. Mex. Cienc. Geol., 23 (2006), 302-319]. Revista
801 Mexicana de Ciencias Geológicas 28, 202.

802 Verma, S.P., Díaz-González, L., 2012. Application of the discordant outlier detection and
803 separation system in the Geosciences. International Geology Review 54, 593-614.

804 Verma, S.P., Cruz-Huicochea, R., 2013. Alternative approach for precise and accurate
805 Student´s t critical values and application in geosciences. Journal of Iberian
806 Geology (in press).

807 Verma, S.P., Guevara, M., Agrawal, S., 2006. Discriminating four tectonic settings: five
808 new geochemical diagrams for basic and ultrabasic volcanic rocks based on log-
809 ratio transformation of major-element data. Journal of Earth System Science 115,
810 485-528.

811 Verma, S.P., Quiroz-Ruiz, A., Díaz-González, L., 2008. Critical values for 33
812 discordancy test variants for outliers in normal samples up to sizes 1000, and
813 applications in quality control in Earth Sciences. Revista Mexicana de Ciencias
814 Geológicas 25, 82-96.

815 Verma, S.P., Díaz-González, L., González-Ramírez, R., 2009. Relative efficiency of
816 single-outlier discordancy tests for processing geochemical data on reference
817 materials and application to instrumental calibrations by a weighted least-squares
818 linear regression model. Geostandards and Geoanalytical Research 33, 29-49.

819 Yan, Z., Wang, Z., Yan, Q., Wang, T., Guo, X., 2012. Geochemical constraints on the
820 provenance and depositional setting of the Devonian Liuling Group, east Qinling
821 mountains, central China: implications for the tectonic evolution of the Qinling
822 Orogenic Belt. Journal of Sedimentary Research 82, 9-24.

823 Zaid, S.M., 2012. Provenance, diagénesis, tectonic setting and geochemistry of Rudies
824 sandstone (Lower Miocene), Warda Field, Gulf of Suez, Egypt. Journal of African
825 Earth Sciences 66-67, 56-71.

826

List of Tables

Table 1. Stratigraphic correlation for the Huayacocotla area (after Morán-Zenteno, 1994).

Table 2. Major element concentrations in weight % for shales of the upper Jurassic Pimienta (PF; El Crucero), lower Jurassic Huayacocotla (HF; Linda Vista), and upper Cretaceous Méndez Formations (MF; near Ilamatlán), Molango region, Hidalgo, Mexico.

Table 3. Trace element concentrations in ppm for shales of the upper Jurassic Pimienta (PF; El Crucero), lower Jurassic Huayacocotla (HF; Linda Vista), and upper Cretaceous Méndez Formations (MF; near Ilamatlán), Molango region, Hidalgo, Mexico.

Table 4. Rare earth element concentrations in ppm for shales of the upper Jurassic Pimienta (PF; El Crucero), lower Jurassic Huayacocotla (HF; Linda Vista), and upper Cretaceous Méndez Formations (MF; near Ilamatlán), Molango region, Hidalgo, Mexico.

Table 5. Results of successive application of ANOVA at 99% confidence level to element concentration data for shales of the upper Jurassic Pimienta (PF), lower Jurassic Huayacocotla (HF), and upper Cretaceous Mendez Formations (MF), Molango region, Hidalgo, Mexico, after separating normally distributed data based on DODESSYS (Verma and Díaz-González, 2012).

Table 6. Range of elemental ratios of shales in this study compared to the ratios in similar fractions derived from felsic, mafic rocks, and upper continental crust.

List of figures

Figure 1. Map showing study areas and locations of the source areas from where the geochemical data are compiled in this study for comparison (map modified after Keppie, 2004). 1. Lawlor et al. (1999), 2. Lopez et al. (2001), 3. Rosales-Lagarde et al. (2005).

Figure 2 Simplified geology map of the study area showing sample locations (map modified from carta Geologica, Direccion General de Geografia del territoria Nacional, scale 1:1,000,000.

Figure 3 Images of thin section of the shale samples. a) Siltstone (Pimienta Formation), b) Argillaceous siltstone (Huayacocotla Formation), c) Laminated ferruginous siltstone (Méndez Formation). Magnification: 100x. Refer text for explanation.

Figure 4 X-ray diffraction patterns of the shale samples. a: Pimienta Formation (sample EC7); b: Huayacocotla Formation (LV1); c: Méndez Formation (IM5).

Figure 5 SEM and EDS spectrum for the shale samples. a: Pimienta Formation (sample EC7); b: Huayacocotla Formation (LV1); c and d: Méndez Formation (IM10 and IM5, respectively). Arrow mark shows the points where the EDS analyses were performed.

Figure 6 Geochemical classification diagram using log (SiO_2/Al_2O_3)-log(Fe_2O_3/K_2O) (after Herron, 1988). PF = Pimienta Formation; HF = Huayacocotla Formation; MF = Méndez Formation.

Figure 7 Multi-element normalized diagram for the shale samples, normalized against average upper continental crust (Taylor and McLennan, 1985). A horizontal line for shale/upper continental crust value of 1 is included for reference.
a) for the upper Jurassic Pimienta Formation (PF)
b) for the lower Jurassic Huayacocotla Formation (HF)
c) for the upper Cretaceous Méndez Formation (MF)

Figure 8 Chondrite-normalized rare earth elements plot. Chondrite normalization values are from Taylor and McLennan (1985). The average upper continental crust (UCC) value is also included for reference (Taylor and McLennan, 1985).
a) for the upper Jurassic Pimienta Formation (PF)
b) for the lower Jurassic Huayacocotla Formation (HF)
c) for the upper Cretaceous Méndez Formation (MF)

Figure 9 A (Al_2O_3) - CN (CaO^* + Na_2O) - K (K_2O) ternary diagram (molecular proportions; Nesbitt and Young, 1982). PF = Pimienta Formation; HF = Huayacocotla Formation; MF = Méndez Formation. [1] This study; [2,3] Taylor and McLennan (1985); [4] Condie (1993). n = number of samples.

Figure 10 Th/Sc versus Zr/Sc bivariate plot (McLennan et al., 1993). The addition of zircon due to sediment sorting and recycling is observed in trend 2. PF = Pimienta Formation; HF = Huayacocotla Formation; MF = Méndez Formation. n = number of samples.

Figure 11 Plot of Eu/Eu^* versus $(Gd/Yb)_{CN}$ for the shales of the Pimienta (PF), Huayacocotla (HF), and Méndez Formations (MF). Fields are after McLennan and Taylor (1991). [1] shales of this study; [2] upper continental

914 crust (Taylor and McLennan, 1985); [3] Proterozoic Huiznopala gneiss
915 (Lawlor et al., 1999); [4] conglomerate-bearing bed of the late Paleozoic Las
916 Delicias Formation, exposed near Las Uvas, Coahuila, northeastern
917 Mexico (Lopez et al., 2001). Refer to Figure 1 for location of the source
918 areas used for comparison. n = number of samples.
919
920 Figure 12 Sc/Cr-La/Y bivariate plot of Bhatia and Crook (1986).

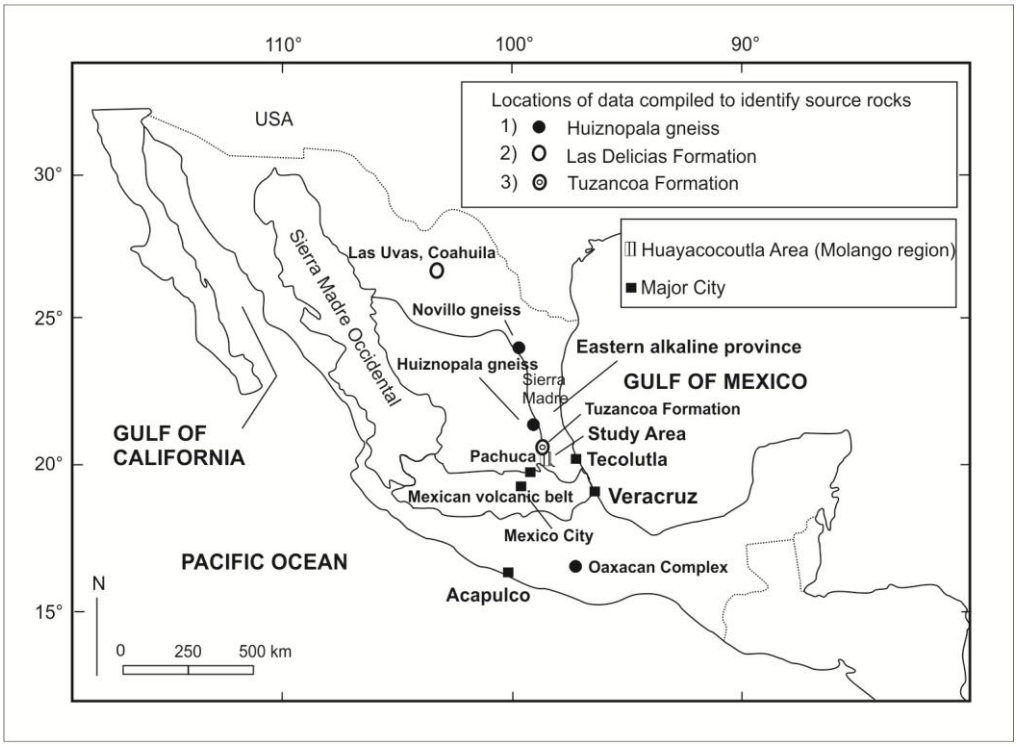
110°
100°
90°
30°
25°
20°
15°
USA
Locations of data compiled to identify source rocks
1) Huiznopala gneiss
2) Las Delicias Formation
3) Tuzancoa Formation
Huayacocoutla Area (Molango region)
Major City
Las Uvas, Coahuila
Novillo gneiss
Huiznopala gneiss
Sierra Madre Occidental
Sierra Madre
Eastern alkaline province
GULF OF MEXICO
Tuzancoa Formation
Study Area
Tecolutla
Pachuca
Veracruz
Mexican volcanic belt
Mexico City
GULF OF CALIFORNIA
PACIFIC OCEAN
Oaxacan Complex
Acapulco
N
0 250 500 km

Fig. 1

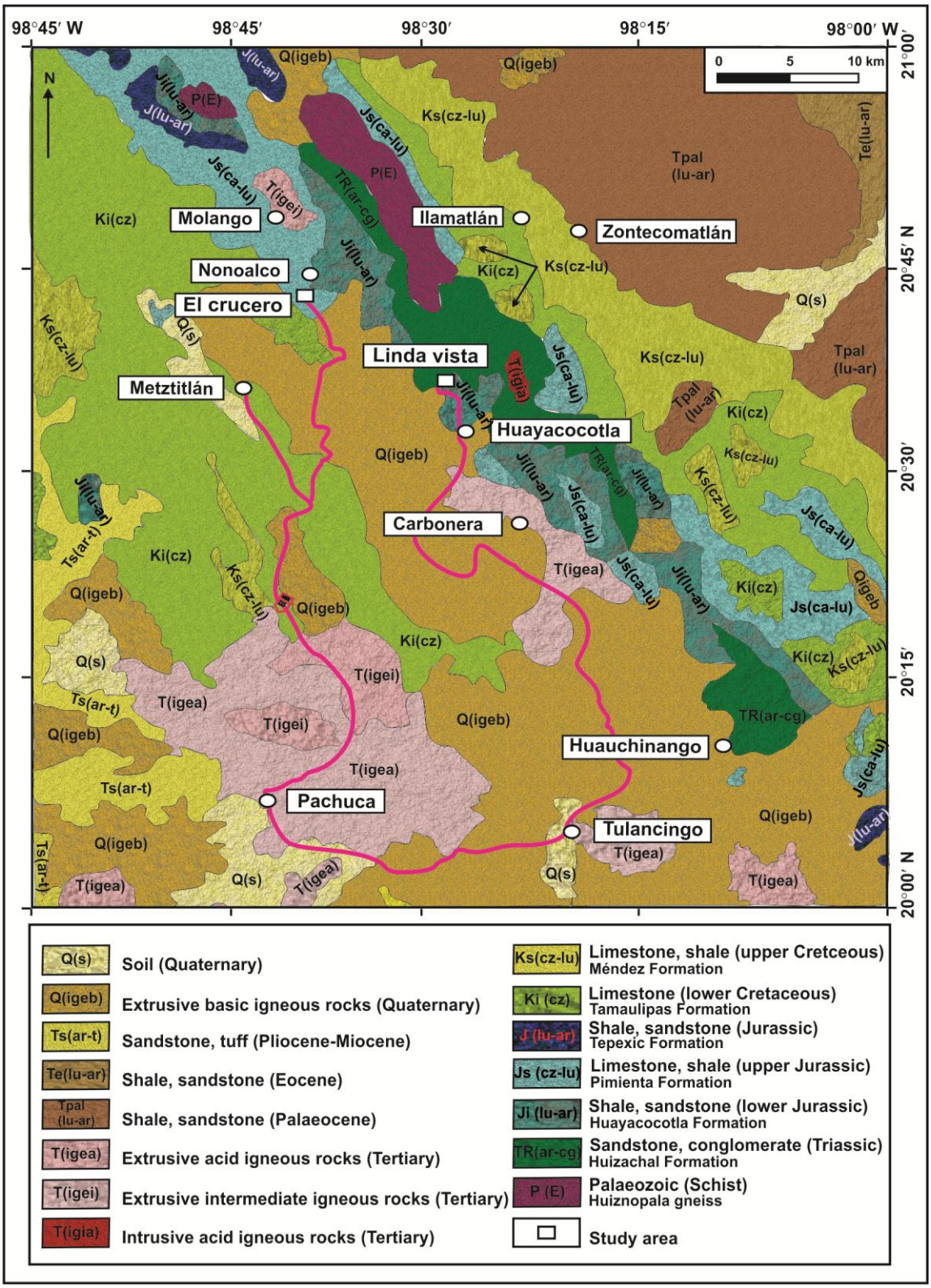
98°45′ W
98°45′
98°30′
98°15′
98°00′ W
21°00′
20°45′ N
20°30′
20°15′
20°00′ N
N
0 5 10 km
Molango
Ilamatlán
Zontecomatlán
Nonoalco
El crucero
Linda vista
Metztitlán
Huayacocotla
Carbonera
Huauchinango
Pachuca
Tulancingo
Q(s) Soil (Quaternary)
Q(igeb) Extrusive basic igneous rocks (Quaternary)
Ts(ar-t) Sandstone, tuff (Pliocene-Miocene)
Te(lu-ar) Shale, sandstone (Eocene)
Tpal (lu-ar) Shale, sandstone (Palaeocene)
T(igea) Extrusive acid igneous rocks (Tertiary)
T(igei) Extrusive intermediate igneous rocks (Tertiary)
T(igia) Intrusive acid igneous rocks (Tertiary)
Ks(cz-lu) Limestone, shale (upper Cretceous) Méndez Formation
Ki (cz) Limestone (lower Cretaceous) Tamaulipas Formation
J (lu-ar) Shale, sandstone (Jurassic) Tepexic Formation
Js (cz-lu) Limestone, shale (upper Jurassic) Pimienta Formation
Ji (lu-ar) Shale, sandstone (lower Jurassic) Huayacocotla Formation
TR(ar-cg) Sandstone, conglomerate (Triassic) Huizachal Formation
P (E) Palaeozoic (Schist) Huiznopala gneiss
Study area

Fig. 2

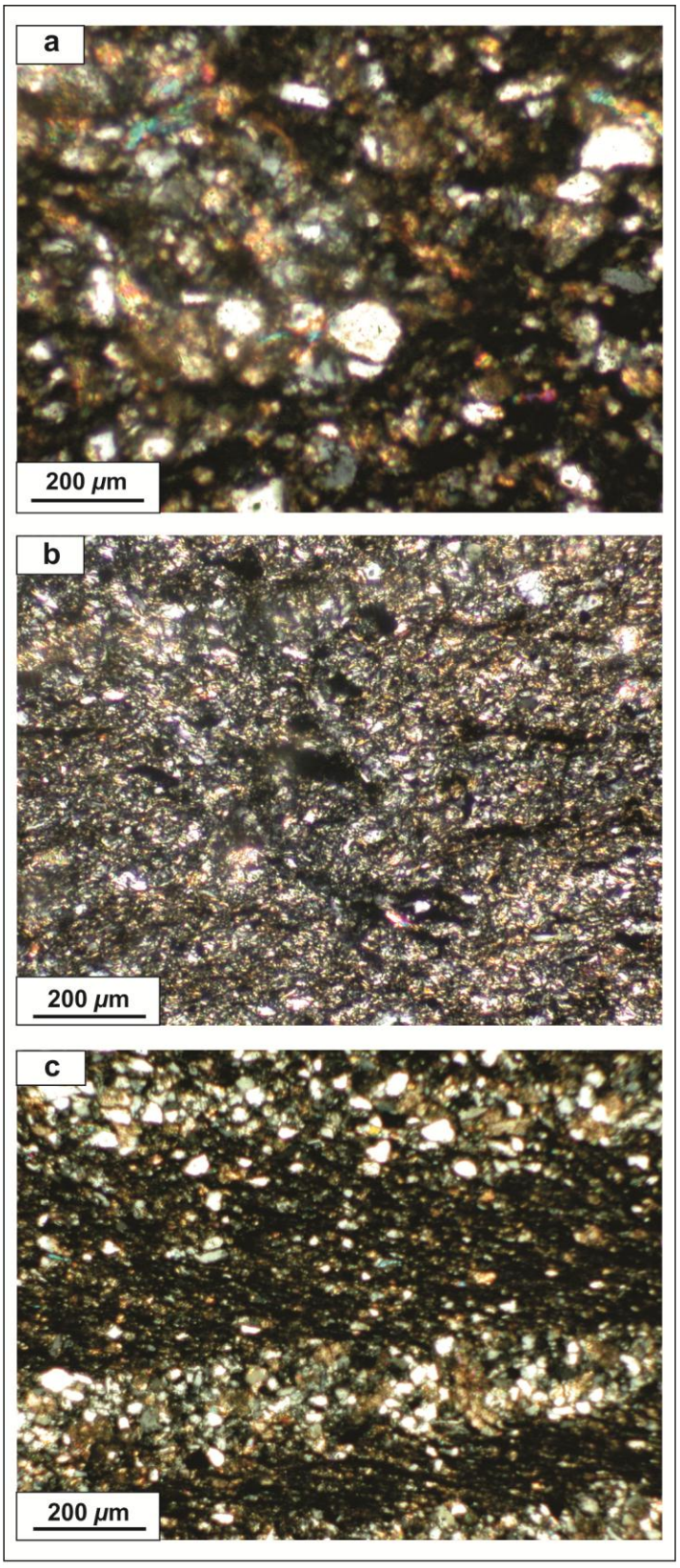

Fig. 3

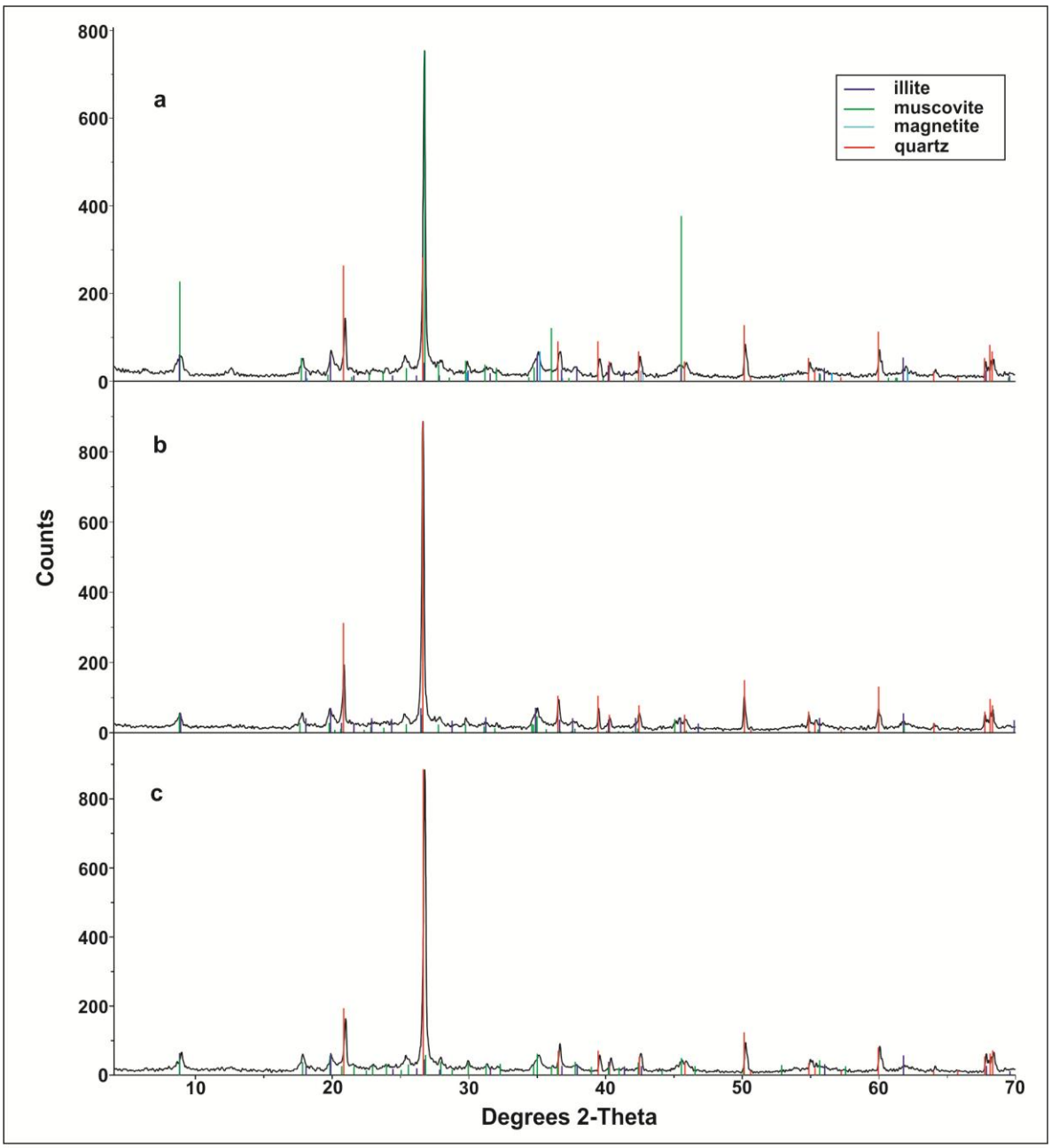
a
b
c
illite
muscovite
magnetite
quartz
Counts
Degrees 2-Theta
0
200
400
600
800
10
20
30
40
50
60
70

Fig. 4

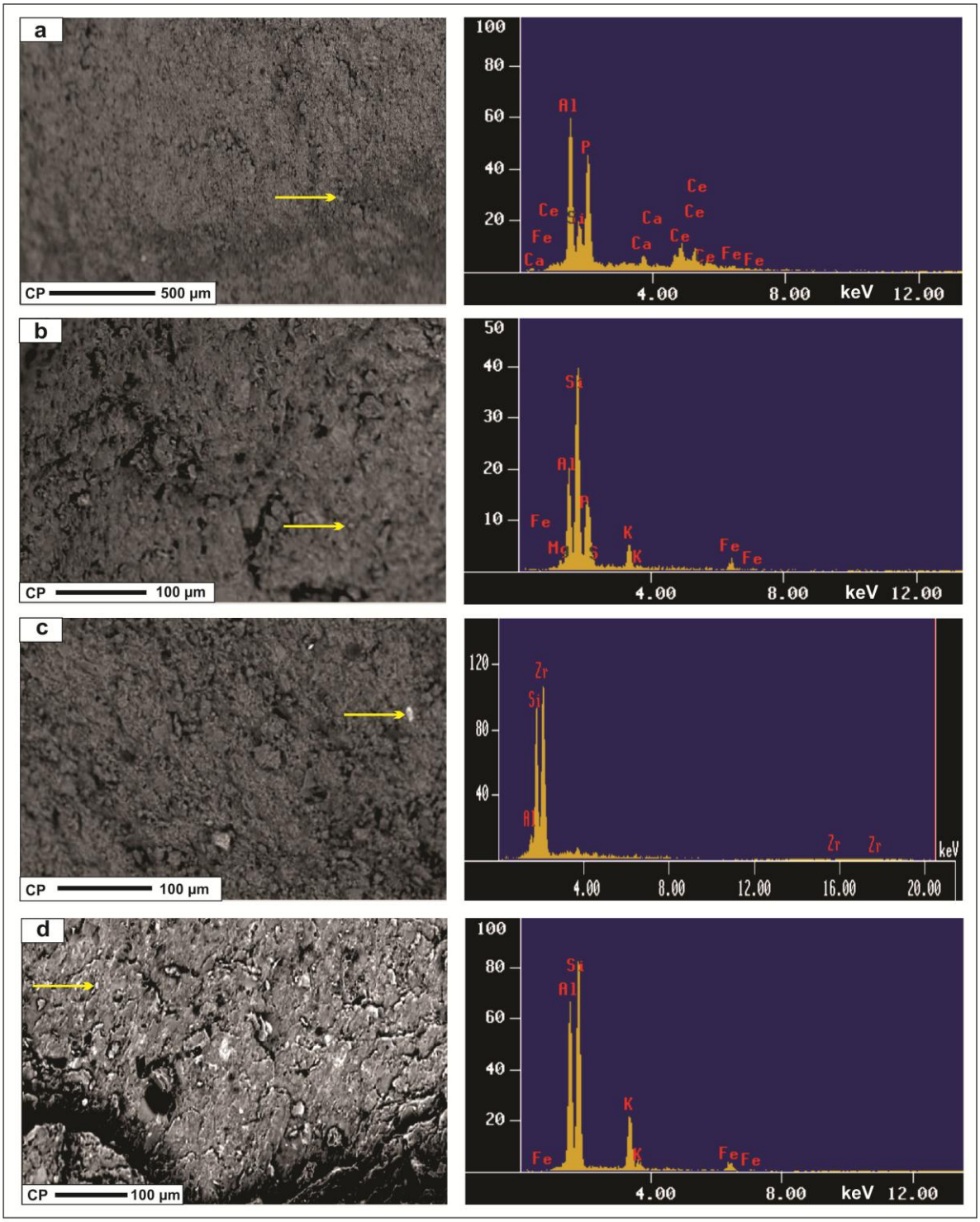
a
CP 500 µm
100
80
60
40
20
Al
P
Ce
Ce
Ca
Ce
Ce
Fe
Ca
Ca
Ce
Ce
Fe
Fe
4.00
8.00
keV
12.00
b
CP 100 µm
50
40
30
20
10
Si
Al
P
Fe
Mg
S
K
K
Fe
Fe
4.00
8.00
keV
12.00
c
CP 100 µm
120
80
40
Zr
Si
Al
Zr
Zr
keV
4.00
8.00
12.00
16.00
20.00
d
CP 100 µm
100
80
60
40
20
Si
Al
K
K
Fe
Fe
Fe
4.00
8.00
keV
12.00

Fig. 5

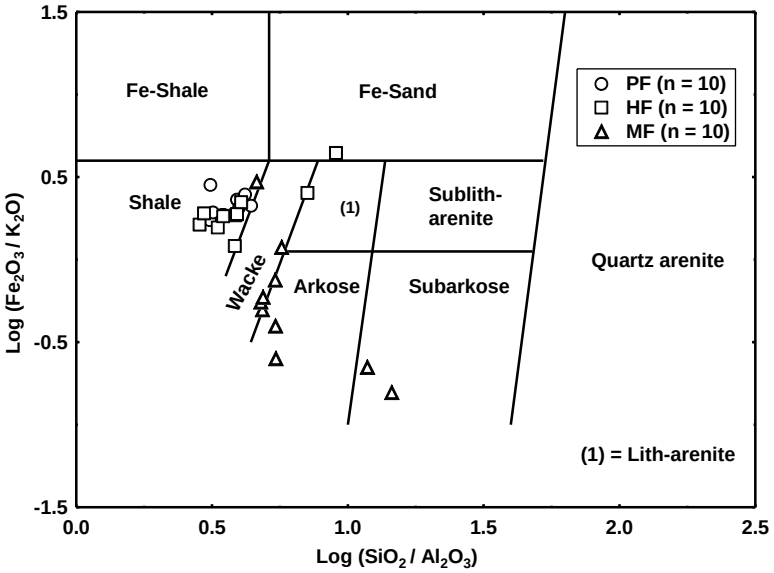
Fe-Shale
Fe-Sand
PF (n = 10)
HF (n = 10)
MF (n = 10)
Shale
(1)
Sublith-
arenite
Wacke
Arkose
Subarkose
Quartz arenite
(1) = Lith-arenite
1.5
0.5
-0.5
-1.5
0.0
0.5
1.0
1.5
2.0
2.5
Log (Fe2O3 / K2O)
Log (SiO2 / Al2O3)

Fig. 6

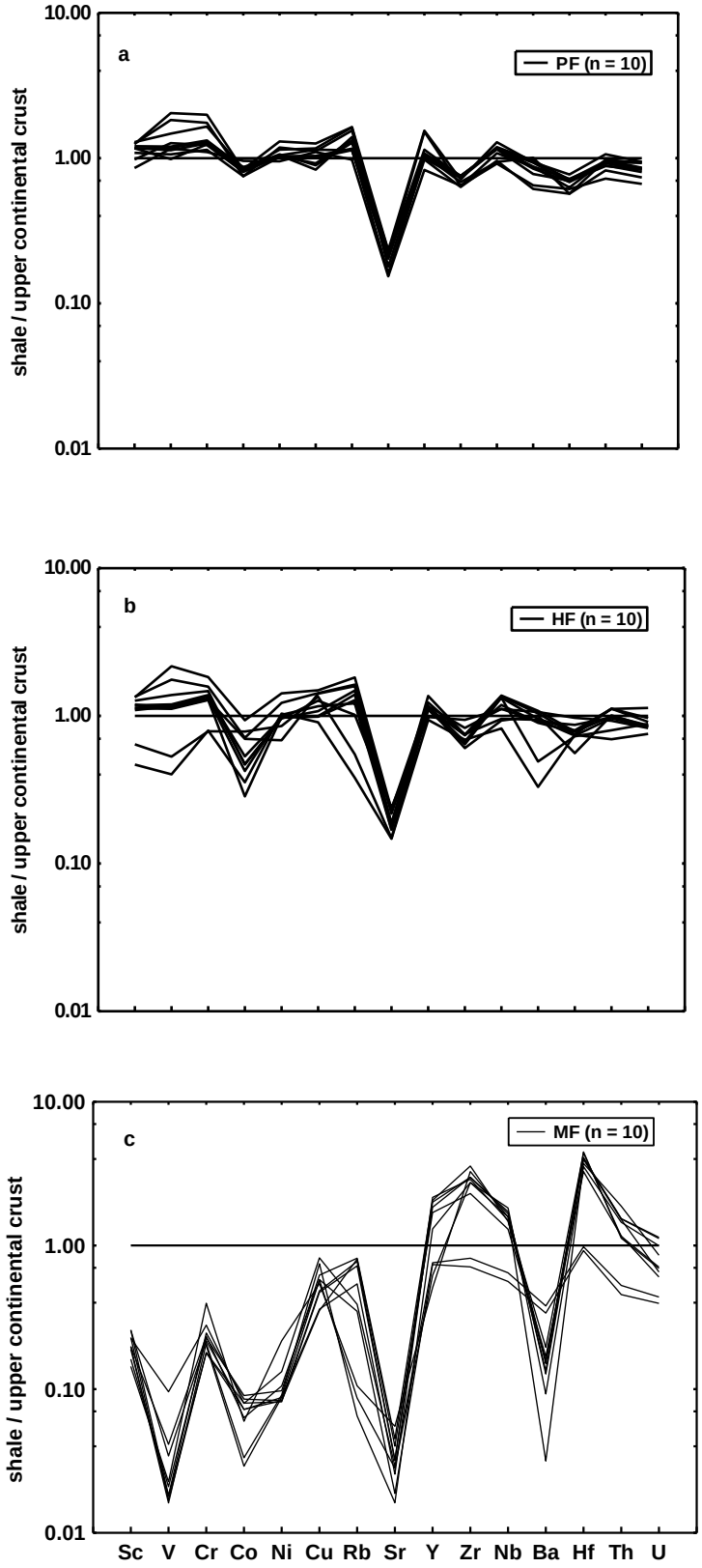
a
PF (n = 10)
b
HF (n = 10)
c
MF (n = 10)
shale / upper continental crust
10.00
1.00
0.10
0.01
Sc V Cr Co Ni Cu Rb Sr Y Zr Nb Ba Hf Th U

Fig. 7

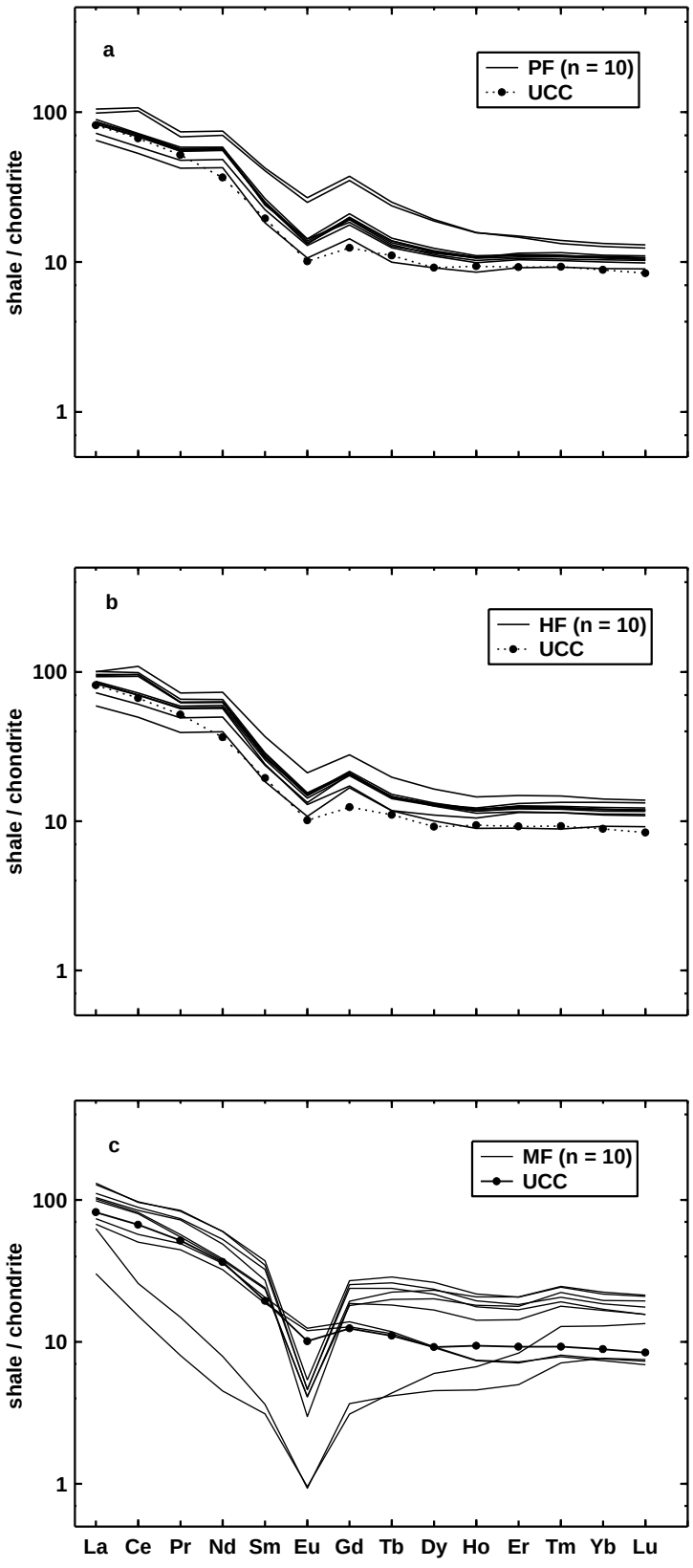
a
PF (n = 10)
UCC
b
HF (n = 10)
UCC
c
MF (n = 10)
UCC
shale / chondrite
100
10
1
La Ce Pr Nd Sm Eu Gd Tb Dy Ho Er Tm Yb Lu

Fig. 8

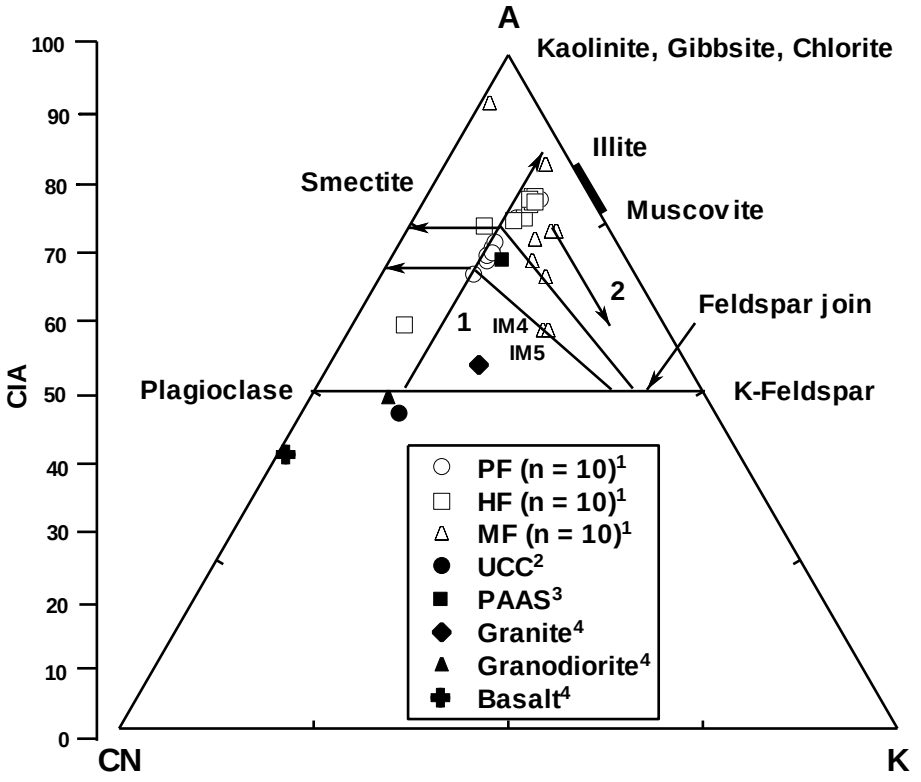
A
Kaolinite, Gibbsite, Chlorite
Illite
Smectite
Muscovite
2
Feldspar join
1
IM4
IM5
Plagioclase
K-Feldspar
CIA
CN
K
100
90
80
70
60
50
40
30
20
10
0
PF (n = 10)[1]
HF (n = 10)[1]
MF (n = 10)[1]
UCC[2]
PAAS[3]
Granite[4]
Granodiorite[4]
Basalt[4]

Fig. 9

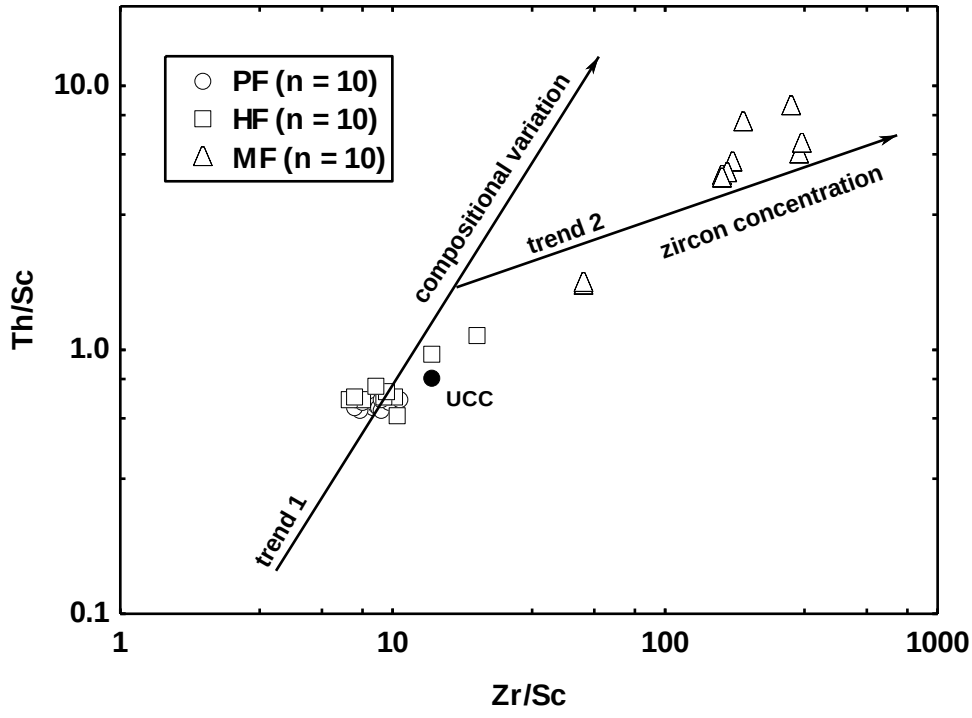
PF (n = 10)
HF (n = 10)
MF (n = 10)
compositional variation
trend 2
zircon concentration
UCC
trend 1
Th/Sc
Zr/Sc
10.0
1.0
0.1
1
10
100
1000

Fig. 10

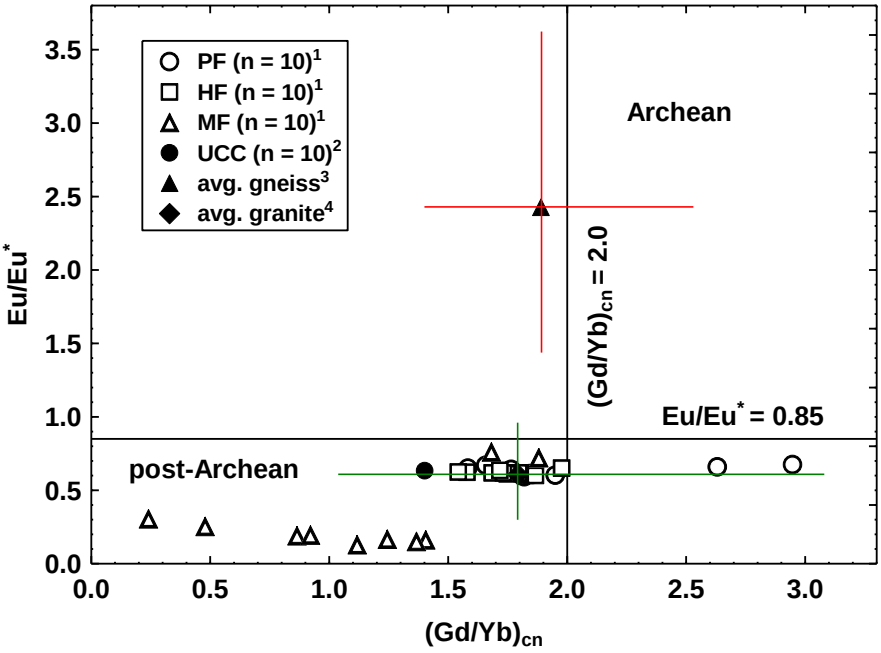
PF (n = 10)[1]
HF (n = 10)[1]
MF (n = 10)[1]
UCC (n = 10)[2]
avg. gneiss[3]
avg. granite[4]
Archean
post-Archean
(Gd/Yb)cn = 2.0
Eu/Eu* = 0.85
Eu/Eu*
(Gd/Yb)cn
0.0
0.5
1.0
1.5
2.0
2.5
3.0
3.5

Fig. 11

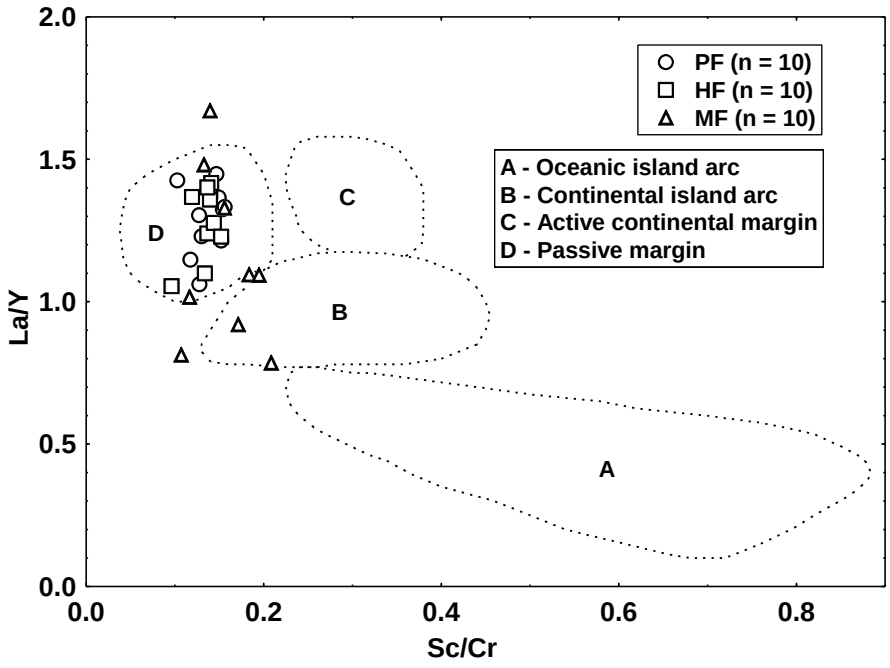
PF (n = 10)
HF (n = 10)
MF (n = 10)
A - Oceanic island arc
B - Continental island arc
C - Active continental margin
D - Passive margin
A
B
C
D
La/Y
Sc/Cr
0.0
0.5
1.0
1.5
2.0
0.2
0.4
0.6
0.8

Fig. 12

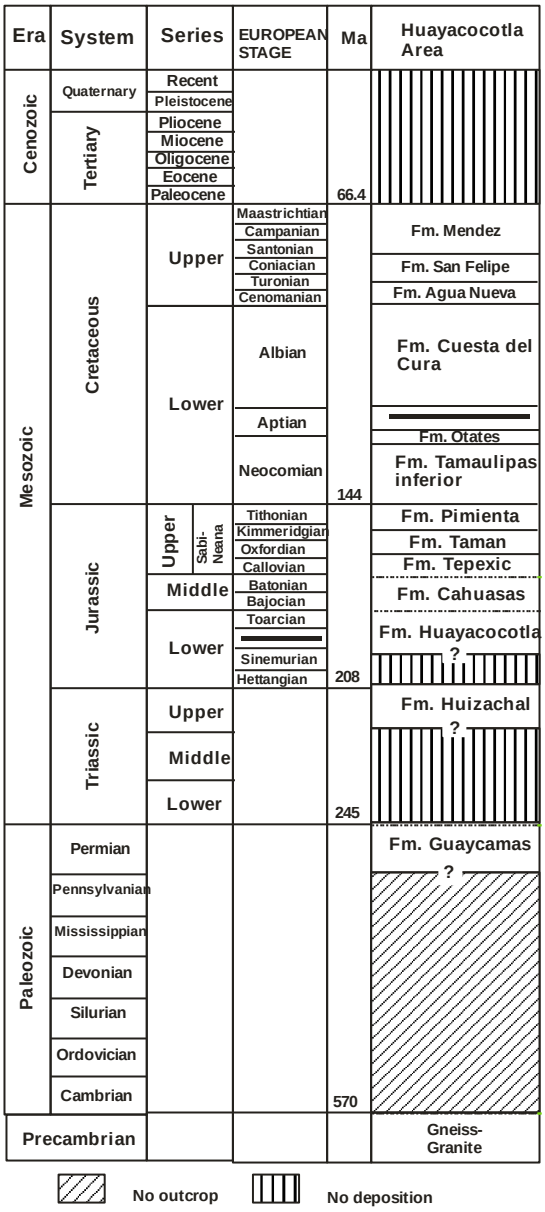

Table 1. Stratigraphic correlation for the Huayacocotla area (after Morán-Zenteno, 1994).

Table 2. Major element concentrations in weight % for shales of the upper Jurassic Pimienta (PF; El Crucero), lower Jurassic Huayacocotla (HF; Linda Vista), and upper Cretaceous Mendez Formations (MF; near Ilamatlán), Molango region, Hidalgo, Mexico.

Location	El Crucero										
Sample #	EC1	EC2	EC3	EC4	EC5	EC6	EC7	EC8	EC9	EC10	Mean±1s (n=10)
vol. free SiO_2	65.70	66.52	66.99	68.79	68.95	65.67	63.12	69.62	71.87	64.60	67.18 ± 2.62
SiO_2	61.30	62.20	62.90	64.80	64.40	61.20	58.70	64.40	67.70	59.50	62.71 ± 2.71
TiO_2	0.90	0.90	0.90	0.90	0.80	0.90	0.80	0.70	0.70	0.90	0.84 ± 0.08
Al_2O_3	18.40	18.10	18.00	16.60	16.20	19.70	18.80	15.40	15.40	18.70	17.53 ± 1.52
$Fe_2O_3^*$	5.50	5.60	5.40	6.00	5.40	5.90	8.50*	6.20	5.10	6.00	5.678 ± 0.363
MnO	0.00	0.00	0.00	0.00	0.10	0.00	0.00	0.00	0.00	0.00	---
MgO	1.20	1.10	1.10	1.00	1.00	0.90	1.20	1.00	0.90	1.10	1.050 ± 0.108
CaO	1.70	1.50	1.60	1.10	1.90	0.20	0.90	1.30	1.00	1.60	1.28 ± 0.50
Na_2O	1.00	0.90	0.90	1.10	0.90	0.80	0.70	0.90	0.90	0.90	0.900 ± 0.105
K_2O	3.10	3.00	2.90	2.60	2.60	3.40	3.00	2.50	2.40	3.10	2.860 ± 0.320
P_2O_5	0.20	0.20	0.20	0.10	0.10	0.20	0.40	0.10	0.10	0.30	0.190 ± 0.100
LOI	6.39	6.12	6.35	5.69	6.03	7.07	6.61	6.94	5.61	6.95	6.38 ± 0.52
Sum	99.69	99.62	100.25	99.89	99.43	100.27	99.61	99.44	99.81	99.05	99.706 ± 0.373
CIA	69.46	70.82	70.51	71.48	67.64	78.61	75.70	70.16	72.31	70.71	71.74 ± 3.18
Al_2O_3/TiO_2	20.44	20.11	20.00	18.44	20.25	21.89	23.50	22.00	22.00	20.78	20.94 ± 1.42
Zr/Al_2O_3	7.63	7.66	7.92	8.62	8.87	6.60	6.51	7.82	7.97	7.24	7.68 ± 0.76
Location	Linda Vista										
Sample #	LV1	LV2	LV3	LV4	LV5	LV6	LV7	LV8	LV9	LV10	Mean
vol. free SiO_2	81.12	63.68	64.17	81.00	68.09	70.16	68.30	70.38	70.69	71.56	70.9 ± 6.0
SiO_2	76.90	58.90	60.00	78.00	63.80	66.30	64.00	66.30	66.80	66.70	66.8 ± 6.3
TiO_2	0.50	0.90	0.90	0.50	1.00*	0.90	0.90	0.90	0.90	0.90	0.811 ± 0.176
Al_2O_3	8.50	20.70	20.30	11.00	19.20	17.20	18.40	17.00	16.50	17.40	16.62 ± 3.92
$Fe_2O_3^*$	4.00	5.70	6.10	3.30	4.70	5.20	5.50	5.30	5.80	3.50	4.91 ± 0.99
MnO	0.10	0.00	0.00	0.00	0.00	0.00	0.00	0.00	0.00	0.00	---
MgO	1.10	1.00	1.10	0.70	0.80	0.90	0.80	0.80	0.80	0.70	0.870 ± 0.149
CaO	1.60	0.70	0.90	0.10	0.10	0.20	0.20	0.20	0.20	0.01	0.42 ± 0.50
Na_2O	1.10	0.90	0.90	1.30	1.00	0.90	0.80	0.80	0.80	1.00	0.950 ± 0.158
K_2O	0.90	3.50	3.20	1.30	3.00	2.80	3.00	2.80	2.60	2.90	2.60 ± 0.83
P_2O_5	0.10	0.20*	0.10	0.10	0.10	0.10	0.10	0.10	0.10	0.10	(0.10)
LOI	4.80	6.93	6.33	3.49	5.96	5.15	5.86	5.43	5.28	6.52	5.58 ± 0.99
Sum	99.61	99.43	99.83	99.79	99.66	99.65	99.56	99.63	99.78	99.73	99.667 ± 0.121
CIA	59.89	75.99	75.52	74.69	79.10	77.92	78.88	78.30	78.59	78.37	75.72 ± 5.77
Al_2O_3/TiO_2	17.00	23.00	22.56	22.00	19.20	19.11	20.44	18.90	18.33	19.33	20.00 ± 2.00
Zr/Al_2O_3	15.39	6.83	6.26	11.08	9.29	9.15	6.24	8.41	8.50	8.13	8.93 ± 2.71
Location	Near Ilamatlán										
Sample #	IM1	IM2	IM3	IM4	IM5	IM6	IM7	IM8	IM9	IM10	Mean
vol. free SiO_2	75.39	75.53	80.60	75.44	76.01	76.53	80.18	80.26	88.97	90.99	80.0 ± 5.7
SiO_2	71.34	72.12	74.40	72.07	71.93	70.60	76.18	75.34	87.01	89.91	76.1 ± 6.8
TiO_2	0.20	0.20	0.22	0.23	0.21	0.36	0.35	0.35	0.36	0.21	0.269 ± 0.075
Al_2O_3	14.73	15.12	16.15	13.32	13.28	14.52	14.09	13.24	7.38	6.21	12.80 ± 3.31
$Fe_2O_3^*$	2.16	2.06	0.47	2.05	1.34	1.90	1.52	2.22	0.39	0.23	1.43 ± 0.79
MnO	0.004	0.004	0.009	0.017	0.016	0.017	0.008	0.018	0.003	0.003	0.010 ± 0.006
MgO	0.269	0.260	0.252	0.536	0.482	0.415	0.479	0.481	0.441	0.383	0.400 ± 0.105
CaO	0.160	0.150	0.089	0.444	0.514	0.198	0.027	0.043	0.035	0.041	0.170 ± 0.174
Na_2O	1.42	1.45	0.53	1.69	1.54	1.03	0.33	0.29	0.39	0.35	0.90 ± 0.58
K_2O	4.31	3.70	0.16	5.14	5.28	3.19	2.00	1.86	1.76	1.45	2.88 ± 1.71
P_2O_5	0.044	0.42*	0.038	0.041	0.051	0.032	0.029	0.045	0.036	0.032	0.039 ± 0.007
LOI	4.32	4.02	6.97	3.57	4.76	5.96	4.83	4.61	2.14	1.45	4.26 ± 1.63
Sum	98.94	99.50	99.28	99.10	99.39	98.20	99.84	98.48	99.94	100.26	99.29 ± 0.64
CIA	66.90	69.41	93.06	59.30	59.11	72.55	83.61	83.80	73.95	73.72	73.54 ± 10.86
Al_2O_3/TiO_2	73.63	75.60	74.06	58.17	64.76	40.90	40.38	37.82	20.67	29.57	1.56 ± 20.15
Zr/Al_2O_3	37.24	37.48	32.28	32.84	51.09	39.07	9.57	11.70	70.56	99.90	42.17 ± 26.76

The abbreviations are: 1s─one standard deviation, and n─total number of samples (n would be less for the parameters for which one or more discordant outliers were detected, see the data identified by an asterisk). See the text for more information. CIA = Chemical index of alteration (Nesbitt and Young, 1982). $Fe_2O_3^*$ = Total Fe expressed as Fe_2O_3.

Table 3. Trace element concentrations in ppm for shales of the upper Jurassic Pimienta (PF; El Crucero), lower Jurassic Huayacocotla (HF; Linda Vista), and upper Cretaceous Mendez Formations (MF; near Ilamatlán), Molango region, Hidalgo, Mexico.

Location	El Crucero										
Sample #	EC1	EC2	EC3	EC4	EC5	EC6	EC7	EC8	EC9	EC10	Mean±1s (n=10)
Ba	530.5	511.7	481.4	466.0	427.5	554.7	480.0	337.5	357.8	516.4	466 ± 72
Cd	0.20	0.29	0.32	0.23	0.55	2.62	0.93	1.50	0.83	0.87	0.83 ± 0.75
Co	14.52	14.75	14.59	14.05	12.78	14.06	12.76	13.67	16.27	14.26	14.17 ± 1.01
Cr	110.0	107.8	104.8	103.3	94.79	165.3	145.3	102.1	91.45	137.1	116.2 ± 24.4
Cs	8.76	8.34	8.02	7.28	7.26	11.44	10.50	8.24	8.00	9.74	8.76 ± 1.38
Cu	20.86	23.05	22.33	28.61	25.13	29.19	27.89	25.94	27.56	31.51	26.21 ± 3.37
Ga	36.44	35.62	34.38	32.98	31.25	37.75	36.33	29.11	28.56	40.09	34.25 ± 3.75
Hf	4.13	3.98	4.17	3.99	4.05	3.30	3.64	3.30	3.55	4.48	3.859 ± 0.393
Nb	14.28	13.90	14.11	13.92	13.82	11.31	13.00	11.52	11.01	15.44	13.23 ± 1.48
Ni	46.10	45.64	46.75	46.02	44.80	50.27	52.07	45.48	41.87	57.37	47.64 ± 4.44
Pb	13.74	15.15	16.82	23.64	28.32	36.81	28.05	29.93	29.36	14.77	23.7 ± 8.0
Rb	156.5	148.2	143.0	126.8	127.3	182.6	173.7	132.2	109.4	183.5	148.3 ± 25.5
Sc	16.45	15.84	15.93	15.92	14.81	17.01	17.07	13.31	11.65	17.53	15.55 ± 1.84
Sr	80.86	76.98	76.01	71.04	75.75	62.68	73.32	56.24	53.78	81.16	70.8 ± 9.8
Th	10.03	9.87	6.67	9.36	9.27	10.13	10.22	8.65	7.59	11.19	9.30 ± 1.34
U	2.38	2.60	2.33	2.24	2.34	2.41	2.62	2.06	1.86	2.65	2.349 ± 0.251
V	128.6	125.9	121.4	105.5	113.6	218.6	196.1	135.7	124.3	158.0	142.8 ± 37.1
Y	22.90	21.88	25.15	23.75	22.95	23.03	33.51	21.57	18.28	34.03	24.7 ± 5.1
Zn	136.7	135.9	113.7	93.73	96.15	279.8	138.1	187.6	158.4	203.9	155 ± 57
Zr	140.4	138.7	142.6	143.1	143.7	130.0	122.4	120.4	122.7	135.3	133.9 ± 9.3
Location	Linda Vista										
Sample #	LV1	LV2	LV3	LV4	LV5	LV6	LV7	LV8	LV9	LV10	Mean
Ba	181.4	595.0	570.6	270.1	584.0	503.0	551.0	517.5	493.3	524.8	479 ± 139
Cd	0.90	0.85	0.54	1.56*	0.50	0.42	0.55	0.42	0.47	4.44*	0.581 ± 0.188
Co	6.03	15.89	12.05	13.31	7.95	9.05	8.02	4.85	7.20	11.87	9.62 ± 3.51
Cr	65.98	152.0	130.0	65.19	122.1	112.7	114.7	106.2	108.9	106.7	108.4 ± 26.4
Cs	2.30	11.12	8.90	3.51	7.43	7.26	7.75	7.52	7.24	9.64	7.27 ± 2.63
Cu	22.61	37.26	35.65	33.68	31.68	24.71	26.90	24.88	29.05	35.33	30.2 ± 5.3
Ga	16.02	44.06	40.99	20.05	37.06	35.85	37.94	35.88	35.45	37.45	34.1 ± 8.9
Hf	4.31	4.54	4.33	4.22	5.62	5.04	3.24*	4.26	4.53	4.62	4.61 ± 0.46
Nb	9.87	16.45	16.24	15.91	13.34	13.40	11.16	11.45	14.21	15.92	13.80 ± 2.37
Ni	45.59	62.45	53.83	37.52	42.28	42.78	42.39	43.53	44.66	30.08	44.5 ± 8.7
Pb	24.29	35.21*	15.57	18.09	13.39	15.59	22.54	14.34	15.18	16.92	17.32 ± 3.73
Rb	42.63	203.6	182.3	61.5	113.8	143.1	166.0	156.2	135.9	177.9	138 ± 52
Sc	6.34	18.16	18.30	8.72	17.23	15.41	16.03	15.30	14.88	16.22	14.66 ± 3.97
Sr	51.51	81.36	76.20	52.05	83.59	64.40	65.33	59.70	59.16	65.29	65.9 ± 11.3
Th	7.30	11.75	11.75	8.38	9.72	10.26	10.58	10.12	10.45	11.69	10.20 ± 1.46
U	2.11	2.71	2.55	2.47	2.32	2.37	2.37	2.36	2.41	3.17	2.484 ± 0.287
V	42.95	232.0	188.2	56.73	148.1	125.3	127.9	119.5	124.1	121.3	129 ± 55
Y	20.66	27.06	25.50	24.23	21.58	25.58	25.15	24.46	24.83	30.02	24.9 ± 2.61
Zn	109.5	154.1	152.1	91.28	121.0	120.9	119.6	134.6	140.4	98.66	124.2 ± 21.2
Zr	130.8	141.3	127.0	121.9	178.4	157.3	114.9	142.9	140.3	141.4	139.6 ± 18.2
Location	near Ilamatlán										
Sample #	IM1	IM2	IM3	IM4	IM5	IM6	IM7	IM8	IM9	IM10	Mean
Ba	83.02	86.73	17.40	92.86	107.7	70.14	186.2	208.9	50.91	73.84	98 ± 58
Co	1.36	1.45	0.57	1.23	1.54	1.23	1.08	1.35	0.50	1.02	1.133 ± 0.352
Cr	14.93	20.43	17.29	14.85	18.90	18.02	19.34	23.19	16.68	32.94*	18.18 ± 2.66
Cs	2.68	2.73	1.18	2.93	2.26	2.36	3.14	3.60	1.20	1.46	2.35 ± 0.83
Cu	11.79	12.08	18.63	8.81	15.56	9.01	14.48	20.50	14.41	13.56	13.88 ± 3.76
Ga	16.77	18.12	15.87	14.2	15.53	16.42	10.12	11.08	13.26	9.39	14.08 ± 3.01
Hf	23.35	23.81	21.65	18.94	25.58	23.05	5.34	5.69	20.53	25.97	19.4 ± 7.6
Nb	17.96	20.00	19.01	15.59	17.66	20.63	6.75	7.75	21.88	18.97	16.6 ± 5.2
Ni	3.59	3.66	4.01	3.65	4.30	3.86	4.63	5.82*	3.87	9.54*	3.946 ± 0.360
Pb	1.52	1.54	0.94	1.18	1.63	1.20	0.96	2.14	1.06	1.10	1.327 ± 0.377
Rb	80.83	86.79	7.28	89.99	91.24	60.57	39.03	43.55	9.71	11.82	52.1 ± 34.5
Sc	3.11	3.50	2.69	2.58	2.20	3.51	2.70	3.08	1.79	1.96	2.71 ± 0.60
Sr	11.15	11.25	5.67	14.05	15.81	8.96	6.58	10.16	9.86	19.32	11.28 ± 4.15
Th	16.14	16.06	19.72	12.21	12.15	15.93	4.78	5.54	15.25	11.80	13.0 ± 4.8
U	3.19	3.13	2.39	1.69	1.98	1.83	1.11	1.23	2.78	1.94	2.13 ± 0.73
V	1.80	1.95	1.73	1.92	2.24	3.67	4.42	10.27*	1.02	2.43	2.35 ± 1.05
Y	47.53	40.60	28.66	37.27	45.32	44.04	16.19	16.69	13.62	11.17	30.1 ± 14.5
Zn	25.98	25.12	35.18	41.18	44.53	50.32	26.63	49.91	10.57	20.01	32.9 ± 13.4
Zr	548.3	566.7	521.2	437.4	678.2	567.3	134.9	154.89	520.7	620.2	475 ± 185

For more information see footnote of Table 2

Table 4. Rare earth element concentrations in ppm for shales of the upper Jurassic Pimienta (PF; El Crucero), lower Jurassic Huayacocotla (HF; Linda Vista), and upper Cretaceous Mendez Formations (MF; near Ilamatlán), Molango region, Hidalgo, Mexico.

Location	El Crucero										
Sample #	EC1	EC2	EC3	EC4	EC5	EC6	EC7	EC8	EC9	EC10	Mean±1s (n=10)
La	31.30	31.68	30.54	31.45	30.58	32.84	38.46	26.52	23.81	36.10	31.33 ± 4.18
Ce	67.51	67.56	65.42	68.15	66.05	68.88	102.27	56.13	50.76	97.36	71.0 ± 16.3
Pr	7.71	7.69	7.50	7.81	7.54	7.99	10.11	6.54	5.78	9.36	7.80 ± 1.23
Nd	40.29	40.41	39.43	41.19	39.74	41.50	53.07	34.33	30.28	49.75	41.0 ± 6.6
Sm	5.82	5.67	5.70	6.10	5.67	5.54	9.78	5.17	4.22	9.39	6.31 ± 1.80
Eu	1.20	1.16	1.15	1.24	1.17	1.24	2.34	1.12	0.93	2.18	1.37 ± 0.48
Gd	6.02	5.86	6.09	6.42	5.93	5.63	11.43	5.41	4.37	10.71	6.79 ± 2.33
Tb	0.802	0.757	0.802	0.836	0.780	0.739	1.456	0.722	0.578	1.373	0.884 ± 0.289
Dy	4.46	4.26	4.53	4.70	4.41	4.36	7.32	4.17	3.48	7.15	4.88 ± 1.28
Ho	0.92	0.87	0.92	0.94	0.90	0.91	1.34	0.84	0.73	1.34	0.971 ± 0.203
Er	2.79	2.63	2.76	2.78	2.69	2.85	3.64	2.57	2.28	3.71	2.87 ± 0.45
Tm	0.43	0.37	0.39	0.39	0.39	0.41	0.47	0.36	0.33	0.50	0.404 ± 0.051
Yb	2.65	2.57	2.71	2.67	2.64	2.76	3.15	2.48	2.24	3.30	2.717 ± 0.307
Lu	0.40	0.39	0.41	0.40	0.40	0.42	0.47	0.38	0.34	0.50	0.411 ± 0.045
LREE	152.6	153.0	148.6	154.7	149.6	156.8	213.7	128.7	114.9	202.0	157.5 ± 29.8
HREE	18.44	17.71	18.61	19.12	18.13	18.08	29.28	16.94	14.35	28.57	19.9 ± 4.9
ΣREE	172.3	171.9	168.3	175.1	168.9	176.1	245.3	146.7	130.1	232.7	178.7 ± 35.0
Eu/Eu*	0.61	0.61	0.59	0.60	0.61	0.67	0.68	0.64	0.65	0.66	0.632 ± 0.032
Th/Co	0.69	0.67	0.66	0.67	0.73	0.72	0.80	0.63	0.47	0.78	0.68 ± 0.092
Th/Cr	0.09	0.09	0.09	0.09	0.10	0.06	0.07	0.08	0.08	0.08	0.083 ± 0.012
Location	Linda Vista										
Sample #	LV1	LV2	LV3	LV4	LV5	LV6	LV7	LV8	LV9	LV10	Mean
La	21.77	37.00	35.39	26.63	30.58	31.71	34.16	31.24	34.78	36.89	32.0 ± 4.8
Ce	47.62	94.79	91.96	58.17	66.93	69.12	89.53	67.13	91.96	104.26	78.1 ± 18.6
Pr	5.39	8.99	8.59	6.75	7.77	8.08	8.55	7.89	8.56	9.90	8.05 ± 1.25
Nd	28.26	46.48	44.79	35.48	40.54	42.48	44.48	41.20	44.73	51.96	42.0 ± 6.5
Sm	4.25	6.63	6.51	5.47	5.57	6.24	6.32	5.97	6.15	8.52*	5.90 ± 0.73
Eu	0.94	1.35	1.32	1.16	1.13	1.31	1.29	1.24	1.31	1.84*	1.228 ± 0.131
Gd	5.12	6.45	6.38	6.29	5.27	6.60	6.41	6.19	6.14	8.53*	6.09 ± 0.53
Tb	0.68	0.84	0.84	0.85	0.68	0.88	0.85	0.82	0.84	1.14*	0.809 ± 0.075
Dy	3.83	4.94	4.90	4.81	4.18	5.04	4.98	4.84	4.87	6.26*	4.710 ± 0.415
Ho	0.76	1.04	1.02	0.94	0.89	1.03	1.03	1.00	1.00	1.24*	0.968 ± 0.092
Er	2.24*	3.28	3.16	2.88	2.85	3.08	3.12	3.02	3.05	3.71	3.128 ± 0.255
Tm	0.32*	0.48	0.45	0.41	0.41	0.44	0.44	0.43	0.43	0.53	0.447 ± 0.038
Yb	2.29	3.31	3.07	2.73	2.77	2.99	2.97	2.89	2.98	3.50	2.950 ± 0.328
Lu	0.35	0.51	0.47	0.42	0.42	0.45	0.45	0.44	0.45	0.53	0.449 ± 0.050
LREE	107.3	193.9	187.2	132.5	151.4	157.6	183.0	153.4	186.2	211.5	166.4 ± 31.6
HREE	15.59	20.84	20.27	19.35	17.47	20.49	20.25	19.62	19.93	25.41*	19.31 ± 1.70
ΣREE	123.8	216.1	208.8	153.0	170.0	179.4	204.6	174.3	207.4	238.8	187.6 ± 34.0
Eu/Eu*	0.61	0.62	0.62	0.60	0.63	0.62	0.61	0.62	0.64	0.65	0.622 ± 0.015
Th/Co	1.21	0.74	0.97	0.63	1.22	1.13	1.32	2.09	1.45	0.98	1.174 ± 0.409
Th/Cr	0.11	0.08	0.09	0.13	0.08	0.09	0.09	0.10	0.10	0.11	0.098 ± 0.015
Location	near Ilamatlán										
Sample #	IM1	IM2	IM3	IM4	IM5	IM6	IM7	IM8	IM9	IM10	Mean
La	36.25	37.36	38.13	40.84	47.01	48.22	27.06	24.73	11.10	23.02	33.4 ± 11.7
Ce	76.46	78.03	80.78	84.82	92.83	91.93	54.69	48.26	14.60	24.69	64.7 ± 27.9
Pr	7.50	7.80	9.90	10.10	11.38	11.56	6.75	6.10	1.10	2.04	7.42 ± 3.61
Nd	26.64	27.34	34.72	37.51	42.74	42.58	25.44	22.93	3.21	5.62	26.9 ± 13.8
Sm	5.44	5.55	6.27	7.47	8.61	8.02	4.76	4.33	0.72	0.84	5.20 ± 2.71
Eu	0.36	0.36	0.26	0.40	0.47	0.40	1.09	1.04	0.08	0.08	0.454 ± 0.348
Gd	5.92	5.52	5.70	7.30	8.27	7.74	4.24	3.90	0.95	1.12	5.07 ± 2.55
Tb	1.30	1.15	1.05	1.38	1.66	1.51	0.68	0.66	0.25	0.24	0.99 ± 0.51
Dy	8.80	7.67	6.39	8.24	10.01	8.95	3.52	3.47	2.29	1.73	6.11 ± 3.07
Ho	1.77	1.54	1.21	1.50	1.85	1.66	0.63	0.63	0.57	0.39	1.18 ± 0.56
Er	5.17	4.43	3.57	4.19	5.15	4.56	1.80	1.77	2.08	1.25	3.40 ± 1.52
Tm	0.88	0.80	0.64	0.68	0.86	0.73	0.28	0.29	0.46	0.25	0.587 ± 0.247
Yb	5.56	4.86	4.14	4.21	5.39	4.60	1.83	1.88	3.21	1.90	3.76 ± 1.46
Lu	0.81	0.74	0.60	0.59	0.80	0.67	0.26	0.28	0.51	0.29	0.555 ± 0.214
LREE	152.3	156.1	169.8	180.7	202.6	202.3	118.7	106.3	30.72	56.21	138 ± 59
HREE	30.21	26.72	23.29	28.12	33.99	30.42	13.25	12.88	10.32	7.17	21.6 ± 9.8
ΣREE	182.9	183.2	193.3	209.3	237.0	233.1	133.0	120.3	41.1	63.51	160 ± 68
Eu/Eu*	0.19	0.12	0.13	0.17	0.17	0.15	0.72	0.76	0.31	0.26	0.298 ± 0.240
Th/Co	11.87	11.08	34.84	9.91	7.90	12.99	4.44	4.10	30.81	11.60	14.0 ± 10.4
Th/Cr	1.08	0.79	1.14	0.82	0.64	0.88	0.25	0.24	0.91	0.36	0.711 ± 0.328

For more information see footnote of Table 2.

Table 5. Results of successive application of ANOVA at 99% confidence level to element concentration data for shales of the upper Jurassic Pimienta (PF), lower Jurassic Huayacocotla (HF), and upper Cretaceous Mendez Formations (MF), Molango region, Hidalgo, Mexico, after separating normally distributed data based on DODESSYS (Verma and Díaz-González, 2012).

Element (% or $\mu g.g^{-1}$)	Total No. of groups	ν_1	ν_2	F_{calc}	F_{crit}	H_0	Regions without significant differences	Regions with significant differences
SiO_2	3	2	27	17.4054224	6.48949	F		Gr1, Gr2, Gr3
Al_2O_3	3	2	27	6.6339906	6.48949	F		Gr1,Gr2,Gr3
Fe_2O_3	3	2	27	65.6481620	6.48949	F		Gr1,Gr2,Gr3
CaO	3	2	27	19.4552911	6.48949	F		Gr1,Gr2,Gr3
MgO	3	2	27	75.8637609	6.48949	F		Gr1,Gr2,Gr3
K_2O	3	2	27	0.1868709	6.48949	T	Gr1,Gr2,Gr3	
Na_2O	3	2	27	0.0682500	6.48949	T	Gr1,Gr2,Gr3	
TiO_2	3	2	27	72.1816976	6.48949	F		Gr1,Gr2,Gr3
P_2O_5	3	2	27	4.1818042	6.48949	T	Gr1,Gr2,Gr3	
CIA	3	2	27	0.7398343	6.48949	T	Gr1,Gr2,Gr3	
Fe_2O_3/K_2O	3	2	27	20.7800785	6.48949	F		Gr1,Gr2,Gr3
SiO_2/Al_2O_3	3	2	27	7.4502583	6.48949	F		Gr1,Gr2,Gr3
Ba	3	2	27	50.2452336	6.48949	F		Gr1,Gr2,Gr3
Co	3	2	27	97.3983734	6.48949	F		Gr1,Gr2,Gr3
Cr	3	2	27	65.0852634	6.48949	F		Gr1,Gr2,Gr3
Cs	3	2	27	35.3230747	6.48949	F		Gr1,Gr2,Gr3
Cu	3	2	27	40.7898926	6.48949	F		Gr1,Gr2,Gr3
Ni	3	2	27	74.364569	6.48949	F		Gr1,Gr2,Gr3
Zr	3	2	27	32.9820669	6.48949	F		Gr1,Gr2,Gr3
Hf	3	2	27	39.6571021	6.48949	F		Gr1,Gr2,Gr3
Nb	3	2	27	2.8133439	6.48949	T	Gr1,Gr2,Gr3	
Nd	3	2	27	7.8641713	6.48949	F		Gr1,Gr2,Gr3
Rb	3	2	27	18.3125655	6.48949	F		Gr1,Gr2,Gr3
Sc	3	2	27	79.2103269	6.48949	F		Gr1,Gr2,Gr3
Sr	3	2	27	35.621795	6.48949	F		Gr1,Gr2,Gr3
Th	3	2	27	3.7332119	6.48949	T	Gr1,Gr2,Gr3	
V	3	2	27	40.1095432	6.48949	F		Gr1,Gr2,Gr3
Y	3	2	27	1.1571739	6.48949	T	Gr1,Gr2,Gr3	
Zr/Sc	3	2	27	35.0858032	6.48949	F		Gr1,Gr2,Gr3
Zr/Al_2O_3	3	2	27	15.8507456	6.48949	F		Gr1,Gr2,Gr3
Cr/Ni	3	2	27	45.6851588	6.48949	F		Gr1,Gr2,Gr3
La/Sc	3	2	27	56.0284574	6.48949	F		Gr1,Gr2,Gr3
La/Co	3	2	27	39.7896966	6.48949	F		Gr1,Gr2,Gr3
Th/Sc	3	2	27	41.4861711	6.48949	F		Gr1,Gr2,Gr3
Th/Co	3	2	27	15.5702655	6.48949	F		Gr1,Gr2,Gr3
Cr/Th	3	2	27	18.022396	6.48949	F		Gr1,Gr2,Gr3
Sc/Cr	3	2	27	0.4694586	6.48949	T	Gr1,Gr2,Gr3	
La/Y	3	2	27	0.1640778	6.48949	T	Gr1,Gr2,Gr3	
$(La/Lu)_{cn}$	3	2	27	1.5791069	6.48949	T	Gr1,Gr2,Gr3	
TREE	6	4	40	0.6441114	4.3748	T	Gr2,Gr1,Gr5,Gr6,Gr3	Gr4
Eu/Eu^*	6	2	27	0.0461363	6.48949	T	Gr6,Gr2,Gr1	Gr5,Gr3,Gr4
$(Gd/Yb)_{cn}$	5	3	31	0.3972441	5.20854	T	Gr1,Gr5,Gr6,Gr2	Gr3

Gr 1 = PF (Pimienta Formation); Gr2 = HF (Huayacocotla Formation); Gr3 = MF (Méndez Formation); Gr4 = andesite (Permian Tuzancoa Formation); Gr5 = gneiss (Huiznopala, Proterozoic); Gr6 = granite (Paleozoic Las Delicias Formation); F = False; T = True. Source data used for comparison for groups Gr4, Gr5, and Gr6 are from Rosales-Lagarde et al. (2005), Lawlor et al. (1999), and Lopez et al. (2001), respectively. Refer to Figure 1, for location of the source areas used for comparison. Subscript $_{cn}$ refers to chondrite-normalized values. An unpblished software UDASYS was used for this application.

Table 6. Range of elemental ratios of shales in this study compared to the ratios in similar fractions derived from felsic, mafic rocks, and upper continental crust.

Elemental Ratio	Range of shales from Molango Region[1]			Range of sediment from felsic sources[2]	Range of sediment from mafic sources[2]	Upper continental crust[3]
	PF	HF	MF			
Eu/Eu^*	0.59-0.67	0.60-0.65	0.13-0.76	0.40-0.94	0.71-0.95	0.63
$(La/Lu)_{cn}$	7.20-8.46	6.46-8.04	2.25-10.68	3.00-27.0	1.10-7.00	9.73
La/Sc	1.90-2.25	1.77-3.42	6.20-21.35	2.50-16.3	0.43-0.86	2.21
La/Co	1.46-3.01	2.00-6.44	18.28-67.37	1.80-13.8	0.14-0.38	1.76
Th/Sc	0.59-0.65	0.56-1.15	1.77-8.51	0.84-20.5	0.05-0.22	0.79
Th/Co	0.47-0.80	0.63-2.09	4.09-34.84	0.67-19.4	0.04-1.40	0.63
Cr/Th	10.22-16.31	7.78-12.94	0.88-4.18	4.00-15.0	25-500	7.76

[1] This study
[2] Cullers (1994), (2000); Cullers and Podkovyrov (2000)
[3] Taylor and McLennan (1985)
PF = Pimienta Formation; HF = Huayacocoutla Formation; MF = Méndez Formation